

Development, Simulation, and Flight Testing of Damage Tolerant Control Laws for the ADAPT™ Winged Compound Helicopter Scaled Demonstrator

Samuel J. Nadell
Aerospace Engineer
U.S. Army Combat Capabilities
Development Command
Aviation & Missile Center
Moffett Field, CA, USA

Tom Berger
Flight Controls Group Lead
U.S. Army Combat Capabilities
Development Command
Aviation & Missile Center
Moffett Field, CA, USA

Alex DiJoseph
Pilot and Program Manager
Piasecki Aircraft Corporation
Essington, PA, USA

Eric Huang
Flight Controls Engineer
Piasecki Aircraft Corporation
Essington, PA, USA

ABSTRACT

Damage tolerant control (DTC) laws were developed for the Adaptive Digital Automated Pilotage Technology (ADAPT™) Winged Compound Helicopter Scaled Demonstrator, a 10% scale version of the Piasecki X-49A, and tested in simulation and flight. The damage scenarios considered include failures of the aircraft's eight redundant actuators: left, right, and aft swashplate servos; Vectored Thrust Ducted Propeller (VTDP) RPM; rudder; left and right flaperons; and elevator. A pseudo-inverse control allocation scheme was used to reallocate control to the remaining actuators based on detection of a failed actuator. The paper covers discussion of the vehicle configuration, flight dynamics, control design, piloted simulation study to evaluate aircraft survivability and failure severity, and flight testing. The results show that DTC improved aircraft survivability and reduced failure severity, as measured by Sullivan Survivability and Integrated Failure Evaluation Scheme ratings, for three of the five damage scenarios tested in the piloted simulation study. Most notably, DTC enabled recovery after a left swashplate servo hardover that was unrecoverable with DTC off. DTC for this damage scenario was successfully tested in flight.

NOTATION

CG	Center of gravity
DOF	Degrees of freedom
GPS	Global positioning system
J	Frequency-domain mismatch cost
LOES	Lower-order equivalent system
$L_{\beta_{1s}}$	Lateral rotor flap stiffness [s^{-2}]
N	Froude scale factor
$M_{\beta_{1c}}$	Longitudinal rotor flap stiffness [s^{-2}]
p, q, r	Angular rates (roll, pitch, yaw)
RC	Radio control
s	Laplace-domain variable
SCAS	Stability and control augmentation system
τ_f	Rotor flap time constant [s]
ω	Frequency
ζ	Damping

INTRODUCTION

The Adaptive Digital Automated Pilotage Technology (ADAPT™) program, initiated by Piasecki Aircraft Corporation in 2014, has the goal of developing a flight

control software package that will achieve improvements in safety, survivability, performance, and affordability for Vertical Take-Off and Landing (VTOL) aircraft (Refs. 1, 2, 3). ADAPT™ takes advantage of redundant control effectors, which are becoming increasingly common on modern VTOL platforms for applications such as Future Vertical Lift (FVL) and Advanced Air Mobility (AAM), to automatically allocate control to optimize performance during normal flight and reallocate control in response to damage.

The work covered in this paper is part of the ADAPT™ Scaled Demonstrator program, which is focused on demonstrating ADAPT™ technology using a subscale flight-test vehicle based on the Piasecki X-49A. Previous work (Ref. 4) involved system identification of the ADAPT™ Winged Compound Helicopter Scaled Demonstrator at four flight conditions, development of a full flight envelope stitched simulation model (Ref. 5), and comprehensive analysis of the trim and flight dynamics trends with airspeed. The work presented herein is a follow-on effort that covers the development of damage tolerant control (DTC) laws and their evaluation in simulation and flight test. The Scaled

Demonstrator aircraft provides a key advantage in that it allows for rapid flight-test evaluation of the DTC capability.

Previous work by Page (Ref. 6) and Oppenheimer (Ref. 7) provides an overview of various control allocation methods, primarily for application in fixed-wing aircraft. Ivler (Ref. 8) evaluated different control allocation methods for a medium-lift tiltrotor including control ganging, pseudo inverse, and optimization-based methods. Knapp (Ref. 2) and Bridges (Ref. 3) developed and tested various control allocation methods for a full-scale winged compound helicopter based on the Piasecki X-49A in piloted simulation and showed that the pseudo-inverse control allocation method was preferred. Vayalali (Ref. 9) and McKay (Ref. 10) implemented pseudo-inverse control allocation schemes for a simulated compound helicopter and simulated coaxial helicopter, respectively.

A notable contribution of this paper to the existing body of work is the results from flight testing DTC on a real aircraft. This is also a major milestone as it is the first time DTC has been tested in flight for the ADAPT™ program. Additionally, this paper covers the control development and simulation work leading up to the final flight test in considerable detail.

First, a description of the flight-test vehicle, flight dynamics model, implications for damage tolerant control design, and damage scenarios is provided. Next, the control design methodology and results, control allocation variations with airspeed and damage scenario, and practical control design considerations for flight test are discussed. Finally, DTC is evaluated in three sections covering five damage scenarios: (1) offline batch simulations analyzing the effects of each damage scenario, (2) a piloted simulation study evaluating aircraft survivability and failure severity using the Sullivan Survivability Rating (SSR) Scale and Integrated Failure Evaluation Scheme (IFES), and (3) flight-test demonstration of the DTC capability.

FLIGHT VEHICLE DESCRIPTION

This section summarizes key aspects of the flight-test vehicle, flight dynamics model, implications for damage tolerant control design, and damage scenarios considered.

Flight Vehicle Description

The ADAPT™ Winged Compound Helicopter Scaled Demonstrator is a 1:9.62 (approximately 10%) scale version of the Piasecki X-49A; both aircraft are shown in Fig. 1. The Froude scale factor N is determined as the ratio of the main rotor diameters of the Scaled Demonstrator (5.28 ft) and the X-49A (53.75 ft) and is useful for scaling the flight dynamics and control system requirements:

$$N = 9.62 \quad \text{Equation 1}$$

The Scaled Demonstrator leverages the bare airframe of the Align T-Rex 760 commercial RC helicopter, which has a semi-rigid two-bladed main rotor (no stabilizer bar) and was modified to more closely match the X-49A winged compound configuration.

Modifications to the Align T-Rex 760 bare airframe include the addition of (1) carbon fiber wings with flaperons, (2) landing gear, and (3) a fully reconstructed tail. As shown in Fig. 2, the reconstructed tail has an elevator and Vectored Thrust Ducted Propeller (VTDP), a primary feature of the X-49A, which consists of an aerodynamic duct, 13-in-diameter propeller, retractable sector, and rudder at the duct outlet. The rudder and sector are mechanically linked such that both are controlled by the same servo via the rudder/sector fulcrum. A key difference of the Scaled Demonstrator compared with the full-scale X-49A is that the VTDP propeller is controlled by RPM, which is common at subscale due to its lower complexity, instead of collective pitch.

The Scaled Demonstrator has a takeoff weight of 37.65 lb and uses a Pixhawk 4 IMU for flight control. It uses Align DS820M swashplate servos, a Hitec HSB-9380TH servo for the rudder/sector, and MKS HV6130H flaperon and elevator servos.

Table 1 shows actuator position and rate limits, which were obtained during ground tests using an inclinometer and 60 frame/sec camera, respectively. Note that the VTDP RPM control units are % power and the corresponding RPM achieved varies based on battery percentage, temperature, and inflow. The proper instrumentation to measure the VTDP RPM rate limit was not available but could be measured using an optical sensor and reflective tape on the motor (Ref. 11).

Table 1. Actuator Position and Rate Limits

Actuators	Pos. Limits	Rate Limits
Left Swashplate (δ_{spl})	-54 to 28 deg (+ up)	115 deg/s
Right Swash. (δ_{spr})	-28 to 51 deg (+ down)	115 deg/s
Aft Swashplate (δ_{spa})	-53 to 58 deg (+ up)	115 deg/s
VTDP RPM (δ_{rpm})	0-100%	N/A
Rudder (δ_r)	-23 to 64 deg (+ right)	114 deg/s
Left Flaperon (δ_{fl})	-15 to 80 deg (+ down)	124 deg/s
Right Flaperon (δ_{fr})	-15 to 80 deg (+ down)	124 deg/s
Elevator (δ_e)	-15 to 15 deg (+ down)	98 deg/s



Fig. 1. ADAPT™ Scaled Demonstrator (left) and X-49A (right) (Ref. 2).

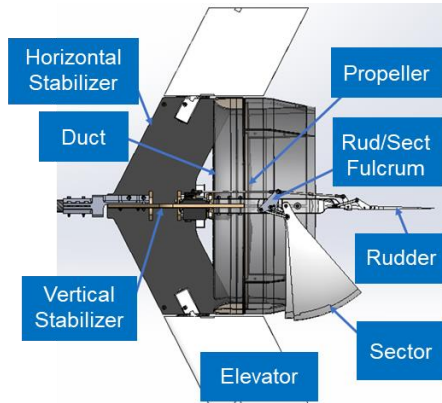


Fig. 2. Vectored Thrust Ducted Propeller (VTDP) component diagram with retracted sector (top view).

Fig. 3 shows select control positions scheduled with *beep*, a pilot control setting used to transition between the aircraft’s hover and forward flight configurations. The pilot adjusts beep using two custom tactile buttons on the back of the FrSky Taranis RC X9D Plus radio control module – the lefthand button decreases beep and the righthand button increases beep. At hover and low speed, a low beep setting is used such that the sector is deflected to direct VTDP thrust in the starboard direction to oppose the torque of the clockwise-spinning main rotor. The flaperons are deflected down to reduce interference with the rotor inflow. At higher speeds, the beep setting is increased such that the sector incrementally retracts to align with the aircraft’s longitudinal axis, and VTDP RPM increases to provide forward thrust and increase airspeed. The flaperons are retracted to reduce drag.

As shown in Fig. 4, a conversion protection system (CPS) was implemented to bound the beep setting within a conversion corridor for all speeds. At low speed, the upper boundary ensures that the sector is extended to direct VTDP thrust starboard to oppose main rotor torque. At high speed, the upper boundary ensures that the forward thrust provided by the VTDP is limited such that the aircraft would not significantly exceed the flight speeds modeled and designed for in this study. The lower boundary limits extension of the sector, which at higher speeds may cause a right yaw moment and the VTDP RPM to drop to its lower limit (0%) to compensate. The Scaled Demonstrator’s conversion protection system provides a similar function to those that manage nacelle angle in tiltrotors such as the Leonardo AW609 and Bell-Boeing V-22 Osprey (Ref. 12).

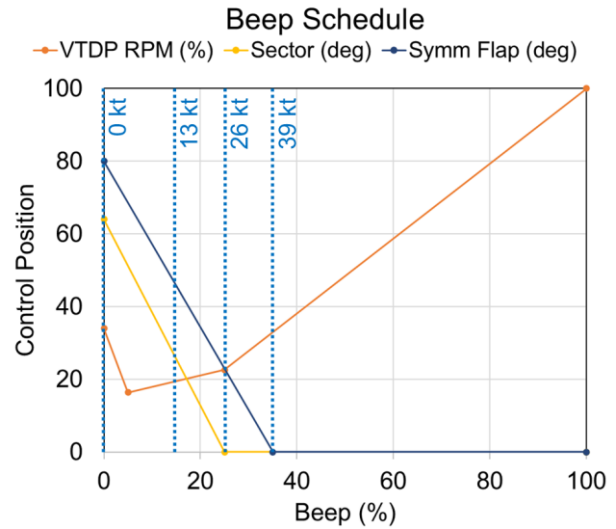


Fig. 3. VTDP RPM, sector, and symmetric flaperon versus beep setting.

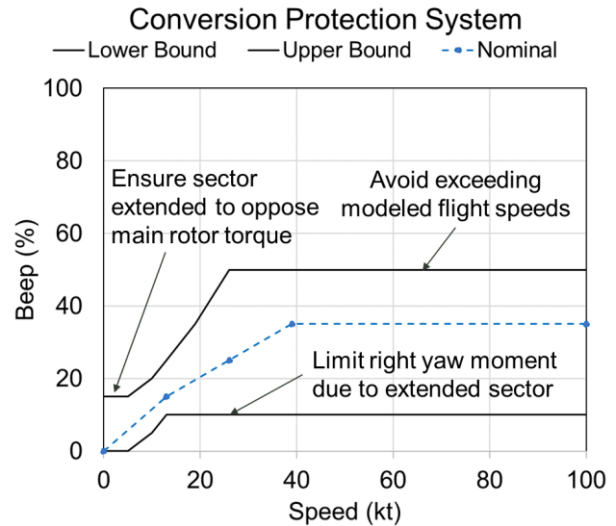


Fig. 4. A conversion protection system was implemented to bound the beep setting within a conversion corridor.

Flight Dynamics Model

In Ref. 4, frequency-domain system identification was performed for the Scaled Demonstrator at four flight conditions spanning its flight envelope (hover, 13, 26, and 39 kt). Based on the identified frequency responses, a quasi-steady hybrid state-space model structure, which explicitly includes the coupled fuselage-rotor flapping dynamics and a first-order model for VTDP RPM lag, was used. State-space models were identified at each flight condition and combined with trim data to form a full flight envelope stitched simulation model (Ref. 5).

As discussed in Ref. 4, the bare-airframe model inputs were defined as eight *virtual effectors*: lateral cyclic (v_1), longitudinal cyclic (v_2), collective (v_3), VTDP RPM (v_4), rudder (v_5), differential flaperon (v_6), symmetric flaperon (v_7), and elevator (v_8). The virtual effectors are groupings of the

individual actuators that were used to concentrate the aircraft response to a primary control axis, which results in higher signal-to-noise ratio and coherence during system identification. The virtual effectors are related to the individual actuators as follows:

$$\begin{bmatrix} v_1 \\ v_2 \\ v_3 \\ v_4 \\ v_5 \\ v_6 \\ v_7 \\ v_8 \end{bmatrix} = \begin{bmatrix} -0.577 & 0.577 & 1 & & & & & & \\ -0.333 & -0.333 & 0.667 & & & & & & \\ 0.333 & 0.333 & 0.333 & & & & & & \\ & & & 1 & & & & & \\ & & & & 1 & & & & \\ & & & & & 0.5 & -0.5 & & \\ & & & & & 0.5 & 0.5 & & \\ & & & & & & & & 1 \end{bmatrix} \begin{bmatrix} \delta_{spl} \\ \delta_{spr} \\ \delta_{spa} \\ \delta_{rpm} \\ \delta_r \\ \delta_{fl} \\ \delta_{fr} \\ \delta_e \end{bmatrix}$$

N

Equation 2

Implications for Damage Tolerant Control Design

Table 2 summarizes the primary axis of response for each virtual effector for the Scaled Demonstrator. It is a key result from Ref. 4 since it indicates the axes and airspeeds where damage tolerant control, which relies on control redundancy, should be evaluated. The table shows that control redundancy exists for roll, pitch, and heave responses at 26 and 39 kt. Note that a vertical response to elevator would typically be expected as in fixed-wing aircraft, but this frequency response and associated control derivative could not be identified with sufficient coherence for the Scaled Demonstrator.

The finding from Table 2 that control redundancy only exists at the higher airspeeds is consistent with previous work (Refs. 2, 3), which involved piloted simulation of damage tolerant control laws using a simulated helicopter based on the Piasecki X-49A. In those studies, for certain damage scenarios, the pilot landed the aircraft above 60 kt since below that speed the redundant aerosurface controls were no longer aerodynamically effective. This full-scale minimum landing speed Froude scales to 19 kt for the Scaled Demonstrator and provides a good estimate of the minimum speed at which the aerosurfaces are sufficiently effective to control the aircraft. This estimate of 19 kt is consistent with the results in Table 2, which shows that the aerosurface responses were sufficiently effective for identification at 26 and 39 kt, but not at hover and 13 kt.

Key challenges for control design for this configuration, which are addressed in this paper, include: (1) scheduling control positions across all airspeeds, (2) highly coupled flight dynamics (particularly due to the VTDP), (3) variable yaw authority during transition to forward flight as the rudder/sector rotates to align with the fuselage, and (4) decreasing control effectiveness of the aerosurfaces, and therefore control redundancy, with decreasing airspeed.

Table 2. Control Redundancy

Virtual Effectors	Primary Aircraft Response by Flight Condition	
	Hover and 13 kt	26 and 39 kt
Lateral Cyclic (v_1)	Roll	
Longitudinal Cyclic (v_2)	Pitch	
Collective (v_3)	Vertical	
VTDP RPM (v_4)	Yaw	Forward Thrust
Rudder (v_5)	None	Yaw
Differential Flaperon (v_6)		Roll
Symmetric Flaperon (v_7)		Vertical
Elevator (v_8)		Pitch

Damage Scenarios

In this study, 39 kt was selected as the primary flight condition for evaluating each damage scenario since it is the highest speed modeled and provides the highest control effectiveness of the redundant aerosurfaces, which are required for DTC. The evaluation will only consider failure of a single actuator at a given time.

Two types of actuator failures are considered in this work. A *lockup* occurs when the actuator gets stuck at its last position at the time of failure. A *hardover* typically refers to the case where the actuator or control surface has moved to its extreme limit. In this study, the definition of hardover is broadened to include any case where the actuator is forced to a specific position (rather than its last position) at the time of failure. This definition is used since, depending on the control effectiveness of the redundant actuators compared to the failed actuator, hardovers to the actuator limit may not be recoverable even with DTC on; thus, various degrees of hardover are considered.

After a comprehensive preliminary evaluation in simulation, the following damage scenarios were selected for detailed investigation:

- Left swashplate hardover and lockup
- Aft swashplate hardover
- Left flaperon hardover
- Elevator hardover

These actuator failures were selected as representative since they correspond to a primary axis of response that has control redundancy: roll, vertical, roll, and pitch, respectively. Note that right swashplate and right flaperon actuator failures were not considered here because their effects are similar to their left-side counterparts. VTDP RPM and rudder failures were not considered since there is insufficient control redundancy in yaw at any given speed due to the rudder being insufficiently effective for control at low speed and the primary effect of VTDP RPM being forward thrust at higher speeds. This work focuses primarily on hardovers since they are the most detrimental type of failure considered and present the most opportunity for improvement with DTC.

CONTROL DESIGN

This section covers the key aspects of the control system architecture, optimization of control system parameters, discussion of the control system stability and performance metrics, and practical considerations for the flight-test implementation of the control laws.

Fig. 5 shows a high-level diagram of the control system, which consists of an explicit model-following (EMF) architecture and control allocation, damage, and damage detection blocks. Control system design parameters were optimized in CONDUIT[®], a flight control design software

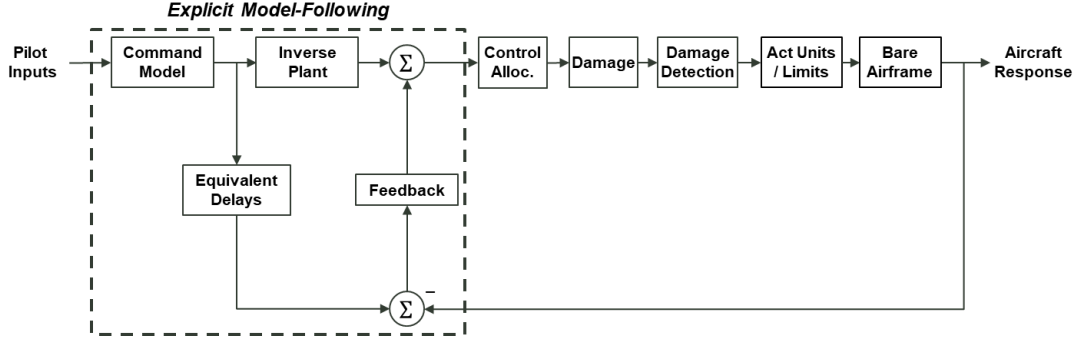


Fig. 5. The control system consists of an EMF architecture and control allocation, damage, and damage detection blocks for testing various damage scenarios.

Explicit Model-Following Control Architecture

Fig. 5 shows that the EMF architecture consists of a command model, inverse plant, equivalent delays, and feedback (Ref. 13). It provides a two degree-of-freedom system that enables independent design of the pilot command response and feedback response (i.e. response to errors and disturbances).

Command Model

The command model determines the response type for each control axis. The lateral and longitudinal command models are second-order transfer functions that are used to obtain an attitude response type (i.e. the pilot commands roll and pitch attitude [deg]):

$$\frac{\phi_{cm}}{\delta_{lat}}, \frac{\theta_{cm}}{\delta_{lon}} = \frac{K_{cm}\omega_{cm}^2}{s^2 + 2\zeta_{cm}\omega_{cm}s + \omega_{cm}^2} \quad \text{Equation 3}$$

The collective and pedal command models are first-order transfer functions that are used to obtain a rate response type (i.e. the pilot commands vertical rate [m/s] and yaw rate [deg/s]):

$$\frac{\dot{h}_{cm}}{\delta_{col}}, \frac{r_{cm}}{\delta_{ped}} = \frac{K_{cm}}{\tau_{cm}s + 1} \quad \text{Equation 4}$$

Parameter $K_{cm} = 30 \text{ deg}, 30 \text{ deg}, 5 \text{ m/s}, \text{ and } 30 \text{ deg/s}$ sets the maximum pilot command for the lateral, longitudinal, collective, and pedal axes, respectively; ω_{cm} and τ_{cm} are set to meet the piloted bandwidth requirements for each axis; and $\zeta_{cm} = 1$ for a critically damped response.

developed by the U.S. Army Combat Capabilities Development Command Aviation & Missile Center (DEVCOM AvMC), at the four key flight conditions (hover, 13, 26, and 39 kt) spanning the aircraft's flight envelope. The EMF command model, inverse plant, equivalent delays, and feedback gains were scheduled with the forward component of GPS ground speed. Airspeed was also considered for gain scheduling but was not selected since the sensor measurement had not been previously validated and was only rated to be accurate from 15-122 kt, which would require transient switching logic to use GPS ground speed at low speed and airspeed at high speed. Trim control positions and control allocation were scheduled with beep.

Inverse Plant

The inverse plant is used to approximately cancel the bare-airframe plant dynamics such that the command model determines the response of the closed-loop system. The lateral and longitudinal inverse plants are modeled as second-order transfer functions representing the coupled rotor-fuselage dynamics:

$$\frac{p}{\delta_{lat}} = \frac{K_{\delta_{lat}}(L_{\beta 1s}/\tau_{f,lat})}{s^2 + s/\tau_{f,lat} - L_{\beta 1s}} \quad \text{Equation 5}$$

$$\frac{q}{\delta_{lon}} = \frac{K_{\delta_{lon}}(M_{\beta 1c}/\tau_{f,lon})}{s^2 + s/\tau_{f,lon} - M_{\beta 1c}} \quad \text{Equation 6}$$

The collective and pedal inverse plants are first-order transfer functions representing the quasi-steady dynamics:

$$\frac{w}{\delta_{col}} = \frac{Z_{\delta_{col}}}{s - Z_w} \quad \text{Equation 7}$$

$$\frac{r}{\delta_{ped}} = \frac{N_{\delta_{ped}}}{s - N_r} \quad \text{Equation 8}$$

The parameter values are obtained by fitting a transfer function to the loop consisting of the control allocation, actuators, and bare airframe, as discussed in Ref. 13. The frequency ranges of the fit were selected about the crossover frequencies for each axis (i.e. the frequencies at which the control system will be active) to ensure good model-following. As will be shown later in Fig. 10, the crossover frequencies for the Scaled Demonstrator are 6.0, 4.0, 7.9, and 1.0 rad/s for the lateral, longitudinal, pedal, and collective

axes, respectively. Fig. 6 shows the lower-order equivalent system (LOES) fit for the lateral inverse plant. The frequency-domain mismatch cost J is well below the guideline $J < 100$, indicating an excellent match (Ref. 13). The fit is also well within the maximum unnoticeable added dynamics (MUAD) bounds, which indicates that the differences would not be perceived by the pilot.

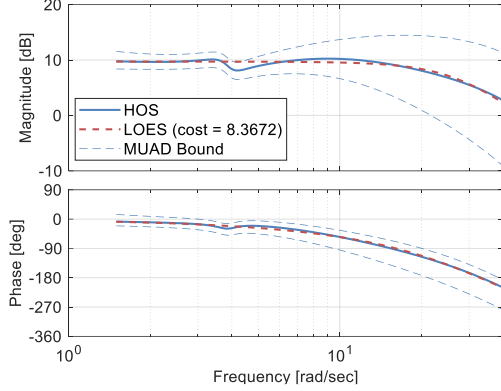


Fig. 6. Lateral axis inverse plant fit.

Equivalent Delays

The equivalent delays are used to synchronize the commanded responses with the measured aircraft responses used for feedback. They are obtained by fitting a time delay $e^{-\tau_{eq}s}$ to the loop consisting of the inverse plant, control allocation, actuators, and bare airframe. Fig. 7 shows an example fit of the equivalent delay for the lateral axis.

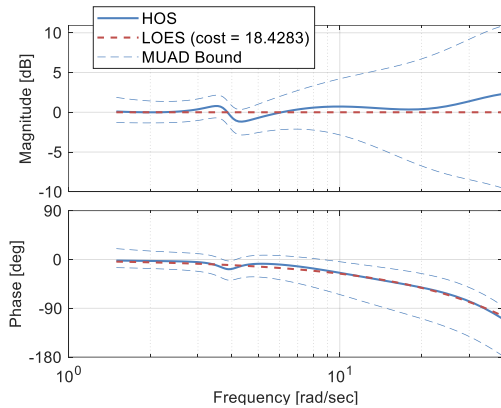


Fig. 7. Lateral axis equivalent delay fit.

Feedback

A typical PID-type architecture is used for the feedback. The feedback architecture was designed to obtain an attitude-command attitude-hold (ACAH) response type for the lateral and longitudinal axes, a rate-command attitude-hold (RCAH) response type for the vertical axis, and a rate-command heading-hold (RCHH) response type for the yaw axis. The feedback gains and other design parameters were optimized in CONDUIT[®] at the four key flight conditions (hover, 13, 26, 39 kt), the results of which will be discussed further in a later subsection.

Control Allocation

Control allocation was used to allocate the control commands for each axis (lateral, longitudinal, vertical, and yaw) to the eight individual actuators.

A buildup approach was used to develop and test the new EMF control system before replacing the legacy mixer and beep schedule, which mitigated risk for flight testing. In the initial (“Baseline”) implementation of the control laws, the control allocation consisted of a 4x4 pseudo inverse upstream of the original mixer developed and previously flown by Piasecki. In this implementation, the pseudo inverse was used to first decouple the control commands for each axis (lateral, longitudinal, vertical, and yaw), then the mixer allocated the decoupled control commands for the four axes to the eight individual actuators. As discussed in Ref. 4, the original mixer consisted of a traditional swashplate mixer with zero phase offset for the lateral, longitudinal, and vertical commands and a transition from using VTDP RPM to rudder for yaw control as beep was increased; no control allocation was made to the flaperons and elevator.

In the final (“DTC”) implementation of the control laws, the 4x4 pseudo inverse *and* original mixer were replaced by an 8x4 pseudo-inverse control allocation scheme that allocates control directly to the eight actuators as required for damage tolerant control. In this implementation, a weighted pseudo-inverse formulation was used that obtains the desired roll, pitch, vertical, and yaw forces and moments \mathbf{d} by allocating control to the actuator commands \mathbf{u}_{cmd} (Refs. 6, 7, 8):

$$\mathbf{u}_{cmd} = \mathbf{W}^{-1} \mathbf{B}_{RB}^T (\mathbf{B}_{RB} \mathbf{W}^{-1} \mathbf{B}_{RB}^T)^{-1} \mathbf{d} \quad \text{Equation 9}$$

where \mathbf{W} is a diagonal weighting matrix and \mathbf{B}_{RB} is the reduced-order 6DOF control effectiveness matrix whose rows correspond to the desired forces and moments (\dot{p} , \dot{q} , \dot{w} , \dot{r}).

Table 3 shows the control effectiveness matrix \mathbf{B}_{RB} used to calculate the pseudo inverse for the nominal (no damage) case at 39 kt as an example. The matrix has been normalized to units of percent actuator throw, which enables weighting to be applied relative to the percentage actuator throw when computing the pseudo inverse. In this study, \mathbf{W} was set to be the identity matrix resulting in equal weighting of the actuators relative to percentage actuator throw.

For each damage scenario, the pseudo inverse is recalculated by zeroing the column of the \mathbf{B}_{RB} matrix corresponding to the failed actuator, which reallocates the control to the remaining control effectors while still achieving the same desired forces and moments. Since \mathbf{B}_{RB} is based on system identification models using flight data and the aircraft has highly coupled, asymmetric flight dynamics, the resulting control effectiveness matrices and control allocations are asymmetric and unintuitive. For example, as shown in Table 3, the left flaperon has a slightly higher control effectiveness than the right flaperon in each control axis (even at 39 kt where the dynamics are expected to be most similar to a fixed-wing aircraft). This is due to the VTDP sector, which even when fully retracted, induces a slight right trim sideslip angle resulting in more lift on the left than right flaperon.

Table 3. Control Effectiveness Matrix (B_{RB}) at 39 kt

	SPL (%)	SPR (%)	SPA (%)	RPM (%)	RUD (%)	FLPL (%)	FLPR (%)	ELV (%)
\dot{p} (rad/s ²)	1.7466	1.3156	-0.4964	0	0	0.6418	-0.5813	0
\dot{q} (rad/s ²)	0.2741	-0.2950	-0.0512	0	0	0	0	-0.0580
\dot{w} (m/s ²)	-0.4316	0.4102	-0.4017	0	0	-0.0444	-0.0402	0
\dot{r} (rad/s ²)	0.0204	0.1540	-0.0970	0.0336	0.1141	0.0512	-0.0464	0

Control Allocation by Flight Condition

The pseudo-inverse control allocation magnitudes across the key flight conditions (0 kt, 13 kt, 26 kt, 39 kt) for the nominal (no damage) case are shown in Fig. 8. Note that, in the control laws, the control allocation was actually scheduled with beep (0%, 15%, 25%, 35%, respectively) rather than speed, but the corresponding speeds are used in this analysis for a more intuitive understanding.

Overall, the control allocation to the flaperons and elevator for each axis is relatively small, meaning that the swashplate actuators provide a more effective control mechanism in the pseudo inverse calculation (even at 39 kt where the aerodynamic effectiveness of the aerosurfaces is highest). This is consistent with the results in Table 3, which show that the swashplate actuators provide greater forces and moments to each axis than the flaperons and elevator. Thus, with the nominal control allocation, the Scaled Demonstrator flies like a traditional helicopter besides the effect of lift forces on the wing and use of VTDP RPM for yaw control at low speed and rudder at high speed. The control effectiveness of the aerosurfaces would be expected to increase with airspeed, but the speed required to match the control effectiveness of the swashplate actuators exceeds the current flight envelope. Decreasing the weighting of the flaperons and elevons in the pseudo inverse would increase their allocation but could also result in undesirable actuator position and rate limiting due to increased actuator activity to compensate for their lower control effectiveness.

Looking more closely at the control allocation for each axis yields some interesting findings. For roll, in addition to the expected allocation to the left and right swashplate servos, there is also allocation to VTDP RPM at 13 kt and rudder at 26 and 39 kt to compensate for roll-to-yaw coupling. For pitch, a large allocation is made to the aft swashplate servo as expected, but greater allocation is made to the right swashplate servo than left and is therefore not symmetric. This provides an effect similar to fine tuning the swashplate phase offset, which was set to zero in the legacy control laws used for system identification. It was noted in Ref. 4, that the non-optimal swashplate phase offset contributed to pitch-roll control coupling during flight testing. For the vertical response, control is symmetrically distributed across the swashplate actuators and VTDP RPM at low speed, then shifts to be dominated by the aft swashplate and rudder at high speed to compensate for heave-to-yaw coupling. For yaw, control allocation shifts from VTDP RPM to rudder due to retraction of the VTDP rudder/sector as expected.

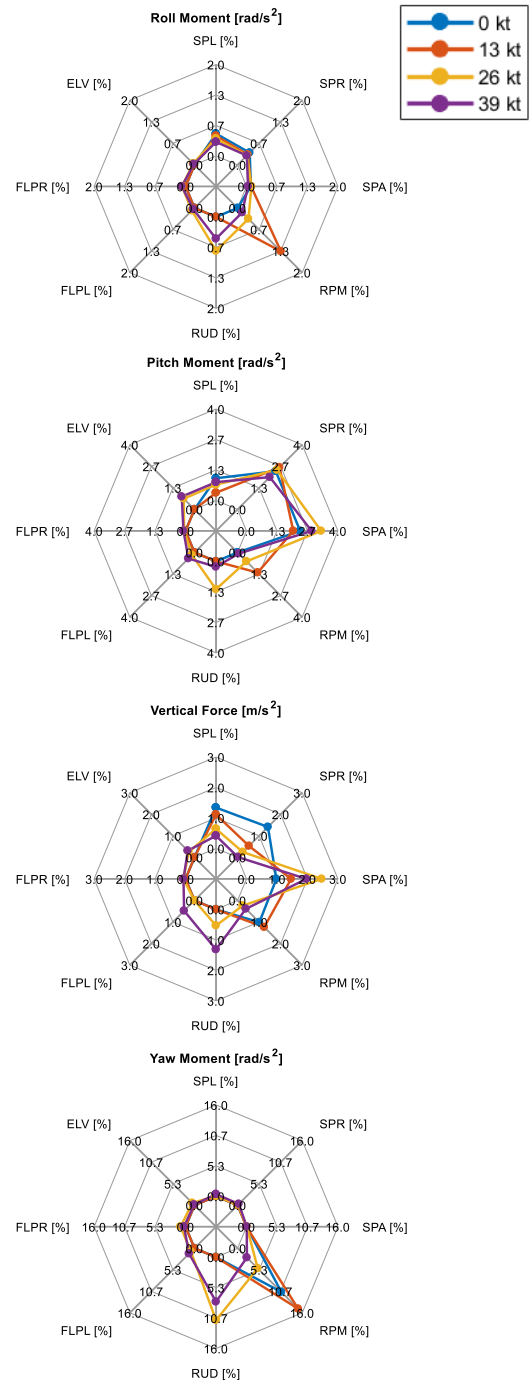


Fig. 8. Nominal pseudo-inverse control allocation magnitudes for various flight conditions.

Control Allocation by Damage Scenario (39 kt)

The pseudo-inverse control allocation magnitudes for each damage scenario at 39 kt – nominal (no damage), left swashplate damage, aft swashplate damage, left flaperon damage, and elevator damage – are shown in Fig. 9. As a result of setting the corresponding column of the \mathbf{B}_{RB} matrix to zero, the allocation to the damaged actuator corresponding to each damage scenario is zeroed and reallocated to the remaining actuators.

For the left swashplate actuator damage scenario (orange line), roll control has a significant reallocation from the left swashplate servo to the flaperons (deflected differentially since the left and right flaperon terms have opposite signs) and rudder. This makes sense since, as shown in Table 3, the flaperons’ largest control effectiveness contributions are for the roll axis. Control allocation to the flaperons and elevator is also slightly increased for the pitch and vertical axes. As will be shown later, this is the scenario for which DTC On shows the most improvement relative to the DTC Off case. It indicates that having effective redundant controls provides good opportunity for damage tolerant control.

For the aft swashplate actuator damage scenario (yellow line), the primary change is that the pitch and vertical control has significantly increased allocation to the elevator and flaperons (deflected symmetrically since the left and right flaperon terms have the same sign). Referring to Table 3, it is observed that symmetric flaperon primarily provides a vertical response and elevator primarily provides a pitch response.

For the left flaperon and elevator damage scenarios (purple and green lines), there is little change to the control allocation. As will be shown later, this indicates that the steady-state impact of damage to these actuators is not significant. Thus, DTC will not provide significant improvement over the nominal control allocation covered in the previous subsection. It will be shown that, similar to the nominal control allocation, the Scaled Demonstrator flies like a traditional helicopter across the full flight envelope (with little use of the flaperons and elevator).

Since there is no control redundancy in yaw (as shown in Table 3), the changes in control allocation for this axis are insignificant for each damage scenario.

Damage and Damage Detection Blocks

Damage and damage detection blocks were implemented in the control laws to simulate the occurrence and response of the control system to damage in simulation and flight test. In this study, hardovers were implemented by commanding the actuator to move to the hardover position at the actuator rate limit, which is the maximum achievable rate of travel without physically modifying or destroying the actuator during flight.

Since actuator positions were not measured, a damage detection block was implemented to measure the difference between the actuator commands upstream and downstream of the simulated damage block. An integrator was used to check if the error between the two signals exceeded a threshold for

a given amount of time (in this case 0.5 sec rather than a shorter time period to avoid spurious false damage detections due to actuator rate limiting). After 0.5 sec of threshold exceedance, a flag would be thrown indicating which actuator had failed, and DTC, if armed, would automatically engage and reallocate control to the remaining actuators.

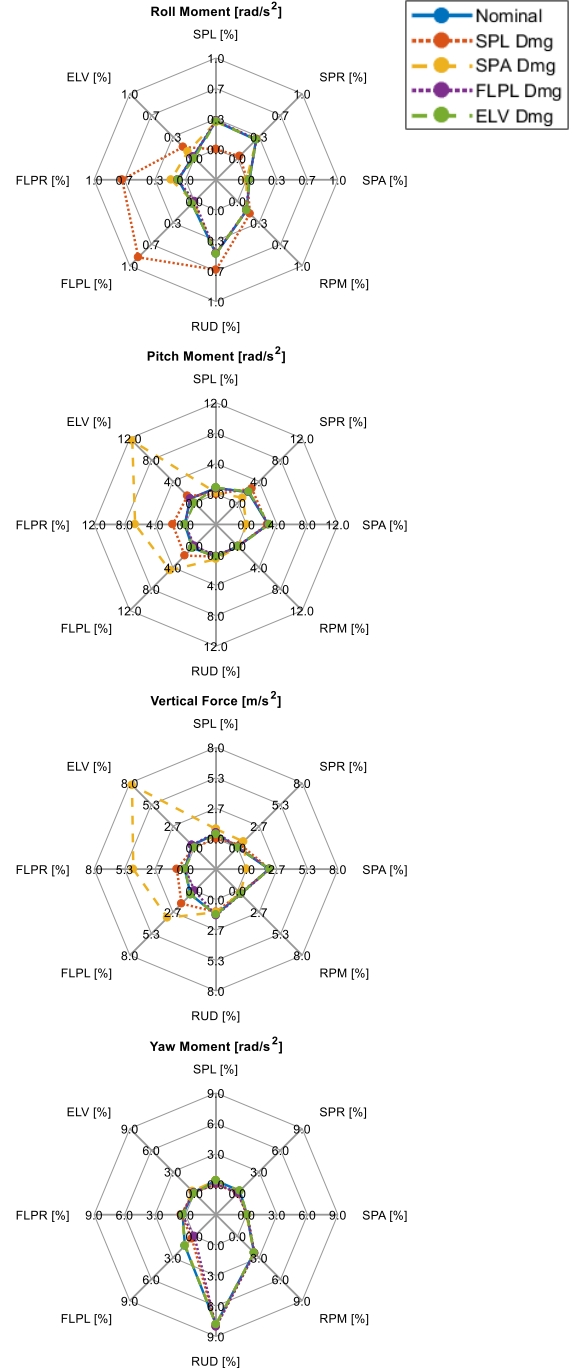


Fig. 9. Comparison of the pseudo-inverse control allocation magnitudes for each damage scenario (39 kt).

Control System Optimization Results

Control system parameters were optimized in CONDUIT[®] using the stability, handling qualities, and control activity specifications listed in Table 4. Many of the frequency-domain requirements were initially Froude scaled relative to the full-scale requirements (using a similar approach to Ref. 14), then adjusted based on the maximum achievable performance for this aircraft. Fig. 10 shows the control system stability and performance results as they appear in CONDUIT[®] where the Level 1 (desired performance) region is shown in blue.

Figures 11, 12, and 13 show key response characteristics for the lateral axis at 39 kt. Figure 11 shows the lateral broken-

loop response, which shows that gain and phase margins meet the requirements of 6 dB and 45 deg, respectively. Figure 12 shows the lateral closed-loop and command model responses in both the frequency and time domains. The responses demonstrate excellent model-following performance, i.e., the aircraft roll attitude response closely tracks the EMF command model in both the frequency and time domains. Figure 13 shows the roll attitude disturbance frequency response, which has a disturbance rejection bandwidth (DRB) of 3.3 rad/sec and disturbance rejection peak (DRP) of 5.0 dB. The disturbance response in the time domain to a 5 deg disturbance in roll attitude is well damped and the excursion magnitude does not exceed 1.5 deg.

Table 4. Control System Optimization Specifications in CONDUIT[®]

Spec Name	Description	Axis	Speed [kt]
<i>Hard Constraints (Stability)</i>			
EigLcG1	Eigenvalues in left-hand plane	All	All
StbMgG1	Stability margin	All	All
NicMgG1	Nichols margin (robust stability)	All	All
<i>Soft Constraints (Handling Qualities)</i>			
ModFoG2	Command model-following cost	All	All
BnwRoH2/F2	Bandwidth and phase delay	R	All
BnwPiH2/F2	Bandwidth and phase delay	P	All
BnwYaH2	Bandwidth and phase delay	Y	All
FrqHeH1	Heave response equivalent time constant, time delay	H	All
CrsMnG2	Minimum crossover frequency	All	All
DrbRoH1	Disturbance rejection bandwidth (DRB)	R	All
DrbPiH1	Disturbance rejection bandwidth (DRB)	P	All
DrbYaH1	Disturbance rejection bandwidth (DRB)	Y	All
DrbPzH1	Disturbance rejection bandwidth (DRB)	H	All
DrpAvH1	Disturbance rejection peak (DRP)	All	All
EigDpG1	Eigenvalue damping	All	All
OlpOpG1	Open-loop on-set point for pilot input (PIO)	All	All
OlpOpG1	Open-loop on-set point for disturbance input (PIO)	All	All
CouPRH1/F1	Pitch-roll coupling (time domain)	R, P	All
CouPRH2	Pitch-roll coupling (frequency domain)	R, P	0
<i>Summed Objective (Control Activity)</i>			
CrsLnG1	Minimize crossover frequency	All	All
RmsAcG1	Minimize actuator activity (RMS) for pilot input	All	All
RmsAcG1	Minimize actuator activity (RMS) for disturbance input	All	All
<i>Check Only</i>			
CouYaH1	Collective-yaw coupling	Y	0

R = Roll, P = Pitch, Y = Yaw, H = Heave

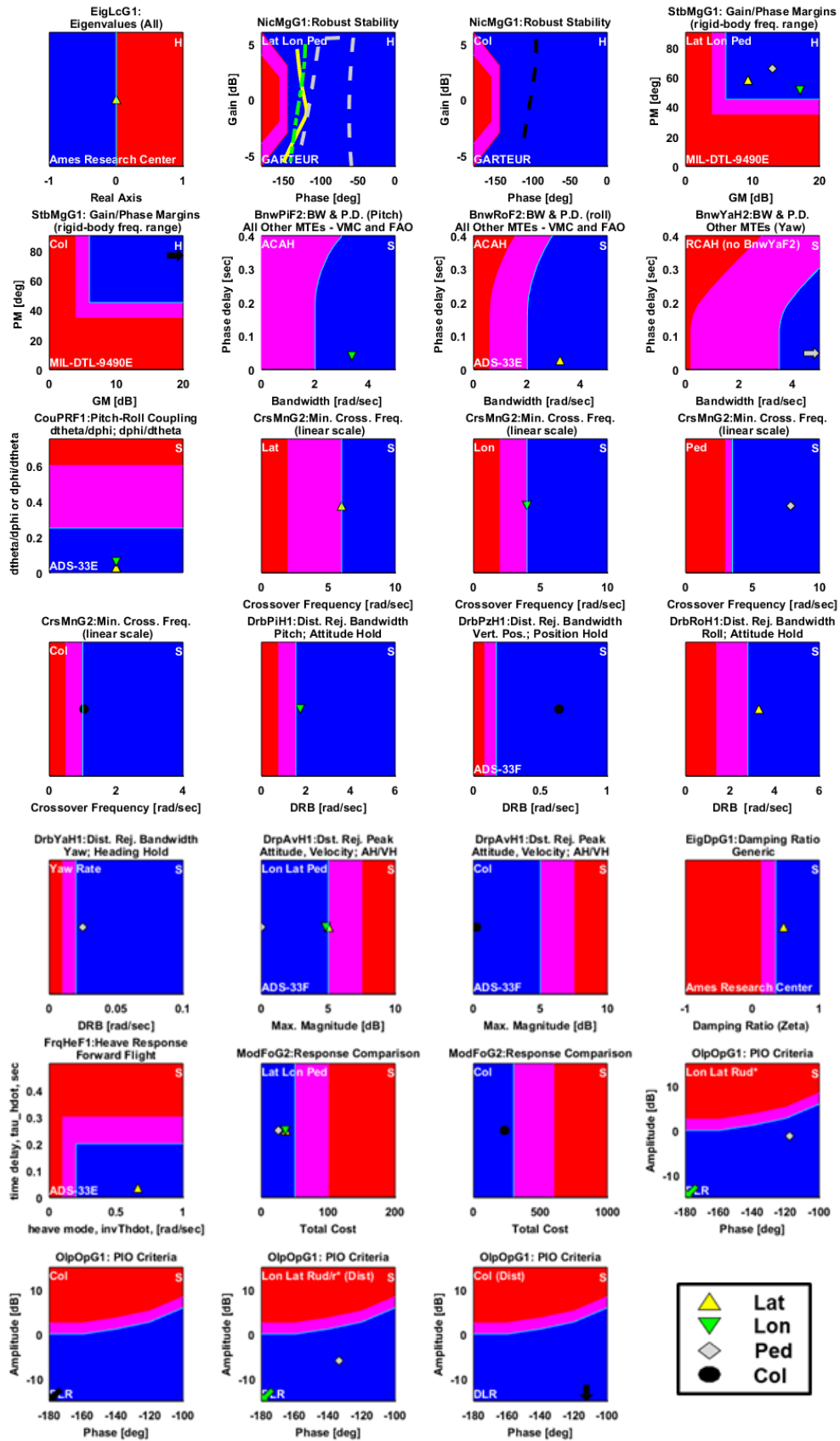


Fig 10. Select specifications used for the 39 kt control system design in CONDUIT® (blue region = Level 1).

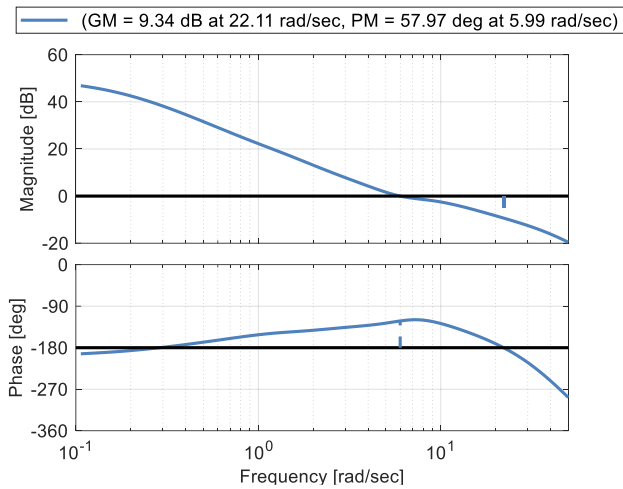


Fig. 11. Lateral broken-loop response (39 kt).

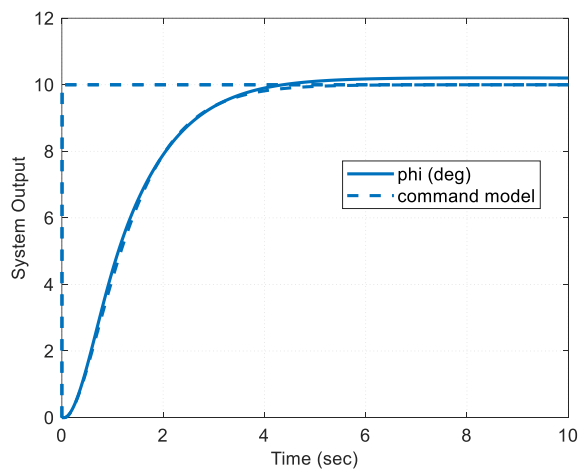
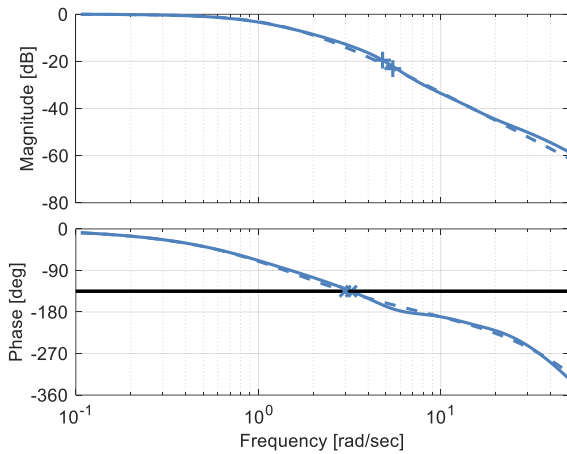


Fig. 12. Lateral closed-loop response in the frequency and time domains (39 kt).

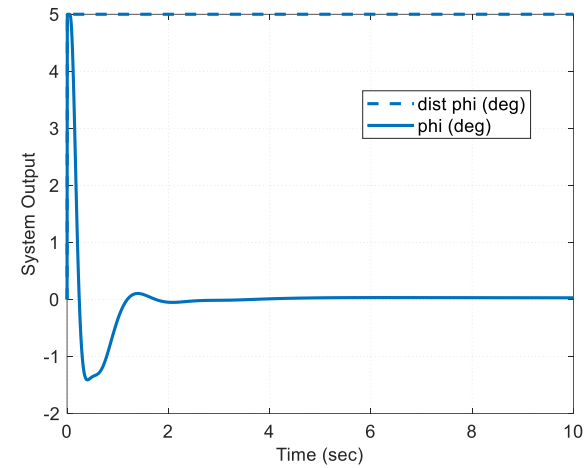
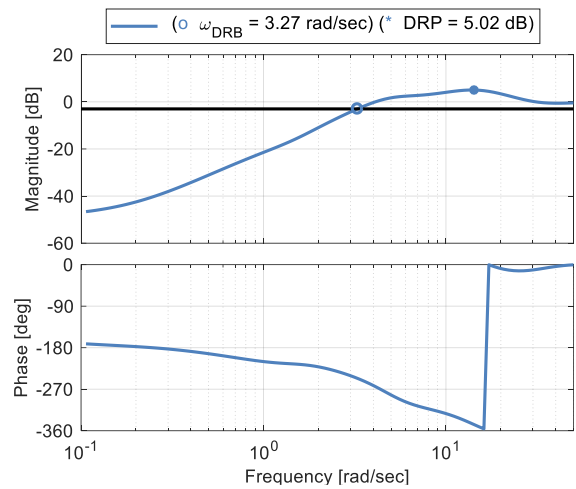


Fig. 13. Lateral disturbance response in the frequency and time domains (39 kt).

Practical Considerations

There were a few practical considerations that required updates to the control laws for flight test. The full flight envelope control laws require considerations for scheduling trim control positions, control allocation, and gains; transient mode switching; anti-windup integrator logic; conversion from continuous to discrete blocks; and other elements and logic not included in the CONDUIT[®] analysis model. It also included input and output handling as required for systems integration ahead of flight test.

Selection of Signals for Control Law Feedback

The new control system was designed to focus primarily on validated signals to mitigate risk for flight test. For example, only the barometric pressure altitude measurement (rather than the unvalidated radar altitude measurement) was used for implementing an altitude hold function, which was only engaged out of ground effect (OGE) to avoid erratic pressure altitude measurements. Similarly, GPS ground speed was used as the sole speed measurement for gain scheduling since the airspeed measurement had not been validated and would require a transient switch to transition between the GPS

ground speed measurement at low speed to the airspeed measurement at higher speeds (since the airspeed sensor was only rated to be accurate from 15-122 kt).

A complementary filter was used to formulate the altitude rate measurement \dot{h} from GPS vertical velocity V_z (low-frequency component) and integrated reconstructed inertial altitude acceleration \ddot{h} (high-frequency component). Reconstructed \dot{h} [m/s²] is formulated as follows:

$$\ddot{h} = a_x \sin \theta - a_y \sin \phi \cos \theta - a_z \cos \phi \cos \theta$$

Equation 10

where a_x , a_y , a_z are the body-axis accelerations at the CG in units of m/s² (Ref. 15).

The complementary filter cutoff frequency was chosen to be 1 rad/sec, as in:

$$\begin{aligned} \dot{h} &= \left(\frac{1}{s+1}\right)(-V_z) + \left(\frac{s}{s+1}\right)\left(\frac{\ddot{h}}{s}\right) \\ &= \left(\frac{1}{s+1}\right)(-V_z) + \left(\frac{1}{s+1}\right)\ddot{h} \end{aligned} \quad \text{Equation 11}$$

and was selected based on the region of high coherence for the GPS vertical velocity V_z signal, as shown in Fig. 14. The GPS V_z measurement is accurate at low frequency (as seen by the high coherence at low frequency) and is used to ensure that biases in integrated \dot{h} do not build up over time.

Prior to flight testing the new control laws, the complementary filter was implemented in the CONDUIT[®] analysis model and validated against system identification flight data captured as part of previous work in Ref. 4 and as shown in Fig. 14 (where v_3 is the collective virtual effector). The results show that the complementary filter accurately synthesizes the two measurements across the frequency ranges where their coherence is highest.

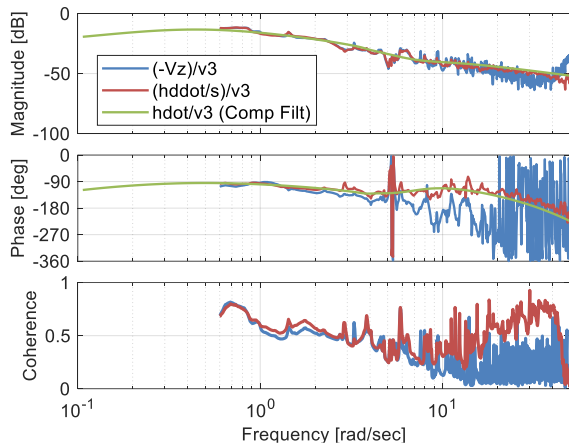


Fig. 14. Validation of the complementary filter using 39 kt system identification data.

Vertical Control

In the new control laws, the pilot's collective controls vertical rate instead of directly controlling collective pitch as in the legacy control laws. Therefore, a 5% dead zone was implemented around the detent collective stick position to

enable the pilot to capture zero vertical rate command more easily.

Aircraft-on-Ground Logic

Aircraft-on-ground logic was used to deactivate all SCAS paths except the rate paths (used for rate damping) to avoid integrator windup on the ground. Since there was no weight-on-wheels sensor for this aircraft to determine when the aircraft was on the ground, a one-time latch was used that would deactivate aircraft-on-ground logic once the pilot collective command exceeded 40% for the first time. The aircraft-on-ground logic would reset (reactivate) once the motor was turned off. The pilot would turn the motor off just after touch down to ensure a smooth landing.

Anti-windup Integrator Logic

Logic was implemented to stop winding up SCAS integrators when any actuator was at the position limit (since the actuators may have effects in multiple axes due to the highly coupled flight dynamics). However, based on tests in simulation, the flaperons and elevator were excluded in this logic since position limiting was a common occurrence during damage scenarios with DTC on (particularly below 26 kt due to lower aerosurface effectiveness) and control authority was still available from the main rotor controls to track the pilot commands.

OFFLINE SIM EVALUATION OF DTC

Simulation provided an effective way to test and evaluate the damage tolerant control capability for a comprehensive set of damage scenarios, including those that are unrecoverable and unsafe to test in flight. Batch offline simulations were run using Simulink and DEVCOM AvMC's RIPTIDE desktop simulation environment for visualization to perform a preliminary evaluation of various damage scenarios that helped inform those to be evaluated in the piloted simulation study and flight test (as will be described in the subsequent sections). The offline simulations generated time histories for each damage scenario that show the transient and new steady-state behavior of the control system and aircraft maneuvering capability. In this section, results for three damage scenarios are shown for the cases of (1) No Damage, (2) Damage (DTC Off), and (3) Damage (DTC On) to evaluate the effectiveness of damage tolerant control at 39 kt. Automated pilot inputs are used to test the controllability of the aircraft in the new steady state for the primary control axis affected by the damage.

Left Swashplate Hardover to 5 deg

Fig. 15 shows the actuator and aircraft responses to a left swashplate hardover to 5 deg. The failure is triggered at $t = 1.0$ sec, then the actuator failure is detected and DTC is automatically engaged 0.5 sec later (for the DTC On case). It is shown that the left swashplate actuator position has a hard drop from its trim position of 10 deg to the 5 deg hardover position (at a rate corresponding to the left swashplate actuator rate limit). For the DTC On case, the hardover induces transient magnitudes of 12 deg roll left, 10 deg pitch down, and 5 m/s vertical descent, which are compensated for by the remaining actuators.

A right roll command of 20 deg at $t = 9.5$ sec is used to test the primary axis of control in the direction opposite the effect of the hardover (more difficult to achieve). With DTC off, the aircraft is unable to recover from the hardover since the left swashplate actuator can no longer be used and control is not reallocated to the remaining effectors. The aircraft enters a divergent roll left that is unrecoverable even with maximum pilot compensation.

This damage scenario demonstrates the most significant improvement DTC On provides relative to the DTC Off case

since it avoids almost immediate loss of the aircraft. The DTC On case accomplishes this by reallocating a significant amount of control to the flaperons. While the right flaperon hits its lower limit of -15 deg, the left flaperon uses its remaining control authority to stabilize the aircraft with a transient deflection of 27 deg. With DTC on, the aircraft is also able to track the commanded roll attitude in the opposite direction and avoid undesirable off-axis responses (e.g. θ , \dot{h} , and r). These DTC On responses closely match the No Damage case.

Note that larger hardovers (e.g. 10 to 0 deg instead of 10 to 5 deg) were unrecoverable even with DTC on. A hardover of this magnitude results in an even larger left roll transient, which may initially be recoverable. However, since the left swashplate servo position is even farther from its trim control position, and the main rotor control effectiveness is significantly greater than that of the redundant aerosurfaces, after several seconds, the left flaperon (the primary remaining redundant aerosurface for the roll axis) will saturate and no longer be able to oppose the left roll divergence. A large hardover in the opposite direction results in an unrecoverable right roll divergence.

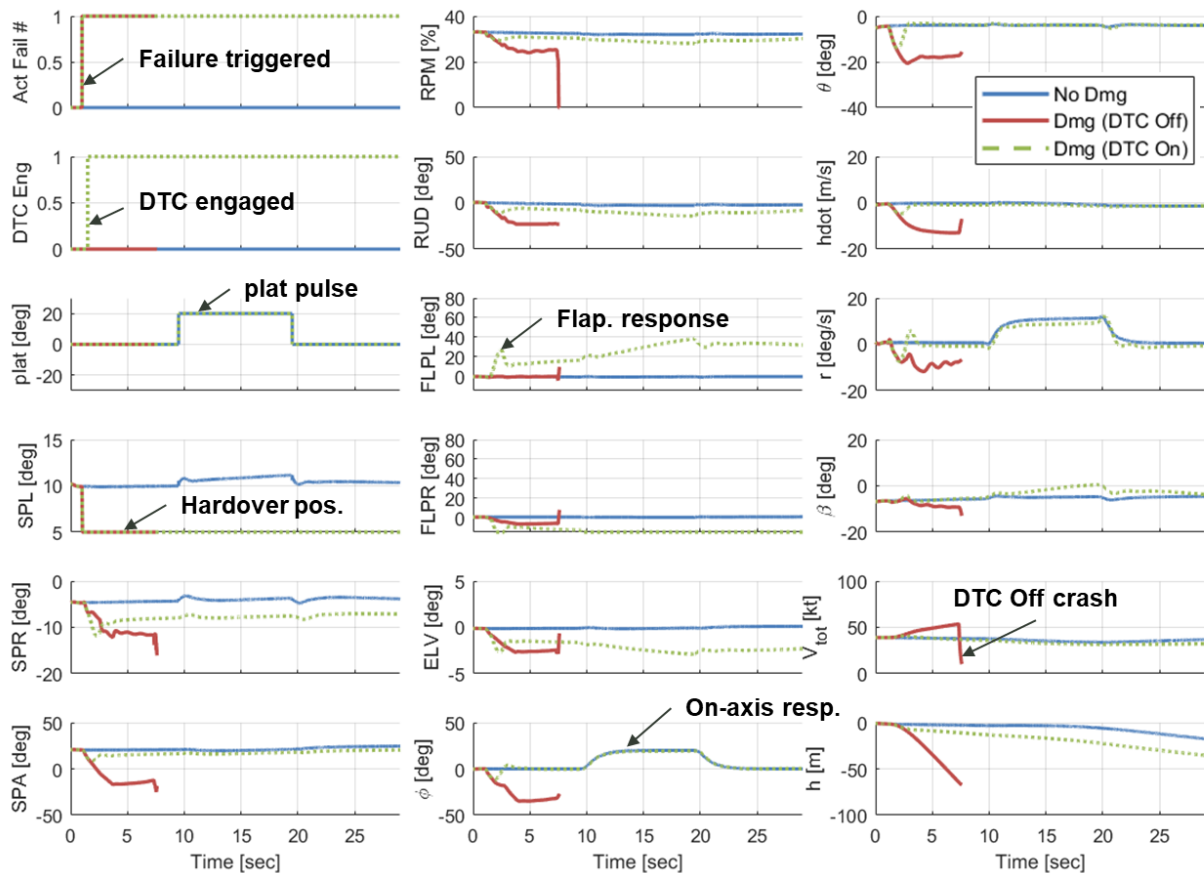


Fig. 15. Actuator and aircraft responses to left swashplate hardover to 5 deg.

Aft Swashplate Hardover to 30 deg

Fig. 16 shows the actuator and aircraft responses to an aft swashplate hardover to 30 deg. The failure is triggered at $t = 1.0$ sec, then the actuator failure is detected and DTC is automatically engaged 0.5 sec later (for the DTC On case). It is shown that the aft swashplate actuator position has a hard drop from its trim position of 20 deg to the 30 deg hardover position (at a rate corresponding to the aft swashplate actuator rate limit). This induces a small transient of about 1 m/s in vertical rate \dot{h} , resulting in a climb that is held in the new steady state.

A vertical rate command of -5 m/s at $t = 9.5$ sec is used to test the primary axis of control in the direction opposite the effect of the hardover (more difficult to achieve). The DTC Off case is not even able to achieve a rate of descent and instead only slightly reduces the rate of climb. This indicates that the aircraft in the DTC Off case has a runaway tendency of increasing altitude and airspeed that could be dangerous and result in loss of the aircraft if not compensated.

The DTC On case is able to achieve an initial descent similar to the No Damage case, but it is still difficult to maintain in

steady state due to the increased aft swashplate hardover position, which results in increased collective. It is able to achieve the descent by full upward deflection of the flaperons and elevator, however, the actuators are at the limits of their control authority. Additionally, the DTC On case reduces off-axis responses in yaw as seen in the yaw rate r and sideslip β responses.

As will be discussed in the piloted simulation study, the pilot would also be able to try other control strategies (e.g. pitching down and reducing beep) to attempt to descend and slow down the aircraft. This helps for the DTC On case, but alone are insufficient to compensate for the climb in the DTC Off case (requires aggressive crabbing).

Similar to the left swashplate actuator hardover, larger hardovers in either direction (resulting in higher or lower collective) are unrecoverable even with DTC On. Higher hardover positions result in a runaway condition of increasing altitude and airspeed. Lower hardover positions result in a high rate of descent to the ground.

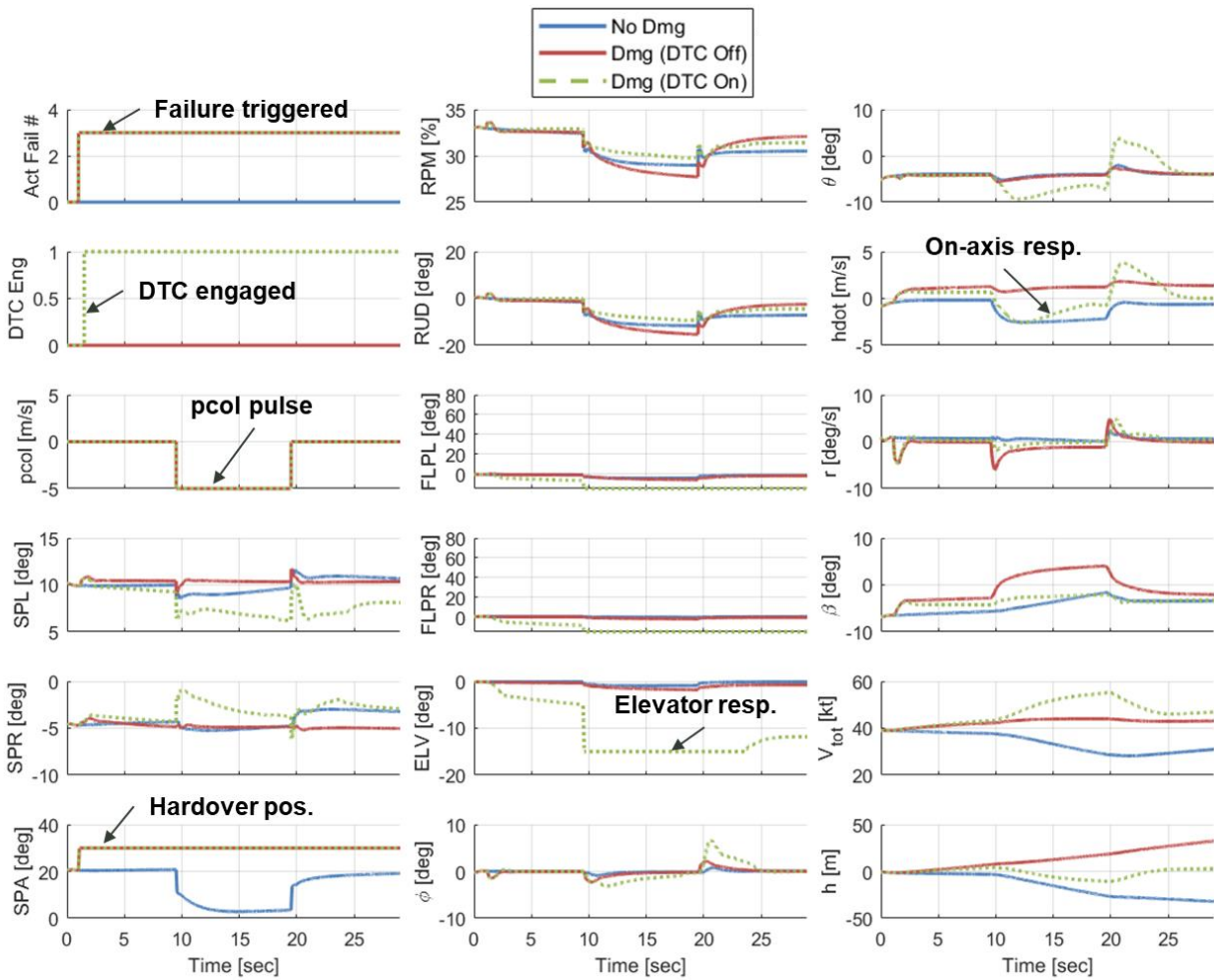


Fig. 16. Actuator and aircraft responses to aft swashplate hardover to 30 deg.

Left Flaperon Hardover to 80 deg

Fig. 17 shows the actuator and aircraft responses to a left flaperon hardover to 80 deg. The failure is triggered at $t = 1.0$ sec, then the actuator failure is detected and DTC is automatically engaged 0.5 sec later (for the DTC On case). The hardover occurs at a rate corresponding to the left flaperon actuator rate limit. The primary effect is a right roll transient of 16 deg and increased drag on the left flaperon in the new steady state, which results in a reduction of speed to 34 kt and increase in sideslip to -16 deg.

After the new steady state is achieved, a left roll command of 20 deg at $t = 9.5$ sec is used to test the primary axis of control in the direction opposite the effect of the hardover (more difficult to achieve). The actuator and aircraft responses for the DTC On and Off cases are almost identical. There is some adjustment to the swashplate servo positions (e.g. the left swashplate actuator has a transient magnitude of 14 deg), but due to their high control effectiveness compared to the aerosurfaces, they are easily able to compensate for the effects

of the hardover. As was discussed in the section covering control allocation, the small difference in behavior between the DTC On and Off cases is consistent with the small change in control allocation for this damage scenario.

After the initial transient, there is little effect on the controllability of the aircraft; it largely flies like a traditional helicopter. Additionally, since flaperon control effectiveness decreases with decreasing speed, slowing down would actually improve the aircraft's flying qualities and a hover landing would be possible.

At significantly higher speeds, it is possible that the same hardover may be more detrimental since the increased aerosurface effectiveness may cause loss of control during the initial transient. This was not examined for this paper since system identification data was not available above 39 kt. Higher flaperon actuator rate limits would also increase the severity of the transient.

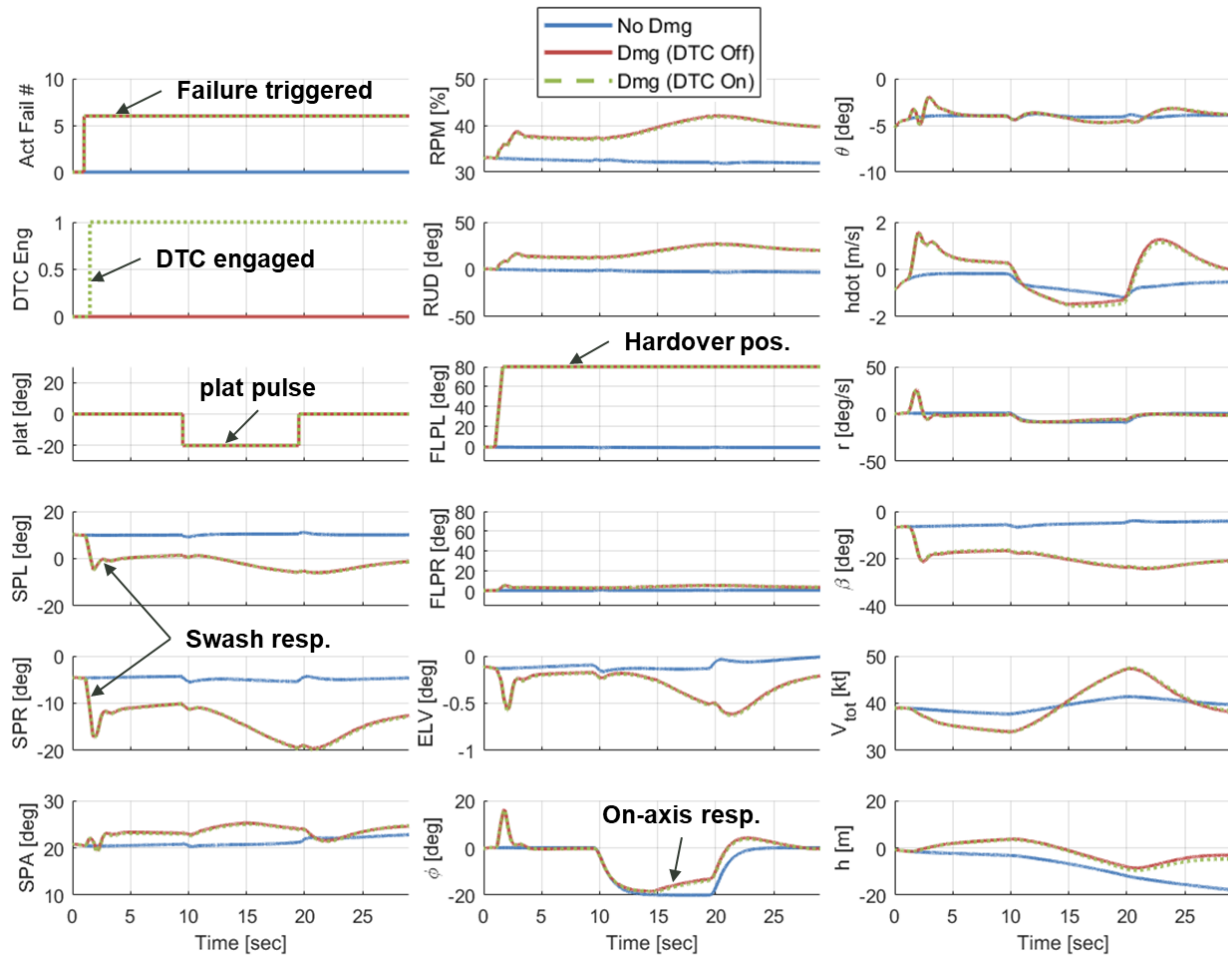


Fig. 17. Actuator and aircraft responses to left flaperon hardover to 80 deg.

PILOTED SIM EVALUATION OF DTC

This section covers the piloted simulation study, which was performed to evaluate aircraft survivability and failure severity, using the Sullivan Survivability Rating (SSR) Scale and Integrated Failure Evaluation Scheme (IFES), during an emergency landing mission for each damage scenario.

Simulation Environment

The piloted simulation study was performed in the Piasecki simulation environment as shown in Figs. 18 and 19. The environment includes the FrSky Taranis RC X9D Plus radio transmitter used for flight test, X-Plane for visualization, the compiled control laws, and the compiled stitched model used for the flight dynamics. A single-point landing gear model with spring and damping terms on vertical position, roll, pitch, and yaw and a braking term on forward speed was used.

Study Setup and Procedure

The pilot performing the evaluation in this study was the Piasecki test pilot for the Scaled Demonstrator who was familiar with the aircraft controls and flying qualities. Since the pilot was already familiar with the selected damage scenarios, the evaluations were not blind. Concerns about biases were reduced since the scales have decision trees with clear conditions associated with each rating (e.g. the SSR Scale specifies the exact aircraft states required to land within the aircraft limits). Additionally, this allowed for thorough evaluation of each damage scenario across multiple test runs and various control strategies where applicable.

Fig. 20 shows the notional landing route used for the emergency landing mission, which was set at Moffett Field, CA, which is the default location for developing and testing control laws in DEVCOM AvMC's RIPTIDE desktop simulation environment. The simulation was initialized at 200 ft and a speed of 39 kt with altitude hold on as would be used for flight test.

The pilot's objective during each test was to land within the aircraft limits. At the beginning of each test, the test conductor set the appropriate DTC (armed or disarmed) and damage scenario settings. The pilot was instructed not to pre-correct for activation of the damage. During the simulation, the pilot used a switch on the radio control to activate the loaded DTC and damage scenario settings. After each test, SSR and IFES ratings were given and pilot comments were recorded.

Rating Scales

Figs. 21 and 22 show the Sullivan Survivability Rating (SSR) Scale (Ref. 2) and Integrated Failure Evaluation Scheme (IFES) (Refs. 16, 17), which were used to evaluate aircraft survivability and failure severity, respectively.

The SSR Scale used in this study was modified to remove wording about injuries to the crew, which was not applicable since the aircraft is unmanned. Additionally, it was noticed in the original SSR Scale, which was used to evaluate a simulated full-scale X-49A in Ref. 2, that the SSR = 3 description was not defined for cases exceeding 1000 ft/min

or 10 deg pitch, roll, and yaw. Thus, the SSR = 3 description was updated to include anything exceeding the nominal aircraft limits (60 kt forward speed, 540 ft/min, 10 deg attitude) for the full-scale X-49A evaluated in that study. Since no in-depth engineering analysis or testing had been performed to determine the aircraft limits of the Scaled Demonstrator, the limits were estimated by Froude scaling the full-scale X-49A aircraft limits in Refs. 2 and 18. Since velocities scale as $1/\sqrt{N}$ and attitudes scale as 1, the estimated aircraft limits for the Scaled Demonstrator used in this study are 19 kt forward speed, 174 ft/min rate of descent, and 10 deg roll, pitch, and yaw. Froude scaling was also applied to all other SSR Scale conditions associated with the aircraft states. Since the full set of missions to be performed by the Scaled Demonstrator is not well defined, the pilot was instructed to give a rating of SSR = 1 if he felt it would be safe to complete another takeoff and landing run.

The IFES provides an alternative, finer resolution scheme that consists of two ratings per test: one for the transient after failure and one for the recovery. In this study, the IFES recovery ratings are focused on the initial *high-speed* behavior after the transient. For some damage scenarios (e.g. left swashplate hardover and lockup), stability and control degraded as speed decreased to 19 kt since the redundant aerosurfaces became less aerodynamically effective. In these cases, the pilot was forced to land at a higher speed to mitigate this degradation and the flying qualities are noted in the comments in Table 5.

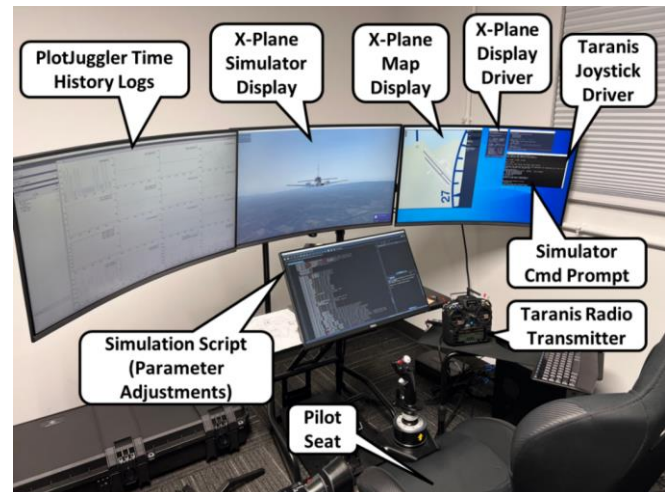


Fig. 18. Piasecki simulation environment.



Fig. 19. The Taranis radio used in the Piasecki simulation environment and flight test.



Fig. 20. Notional route for emergency landing mission.

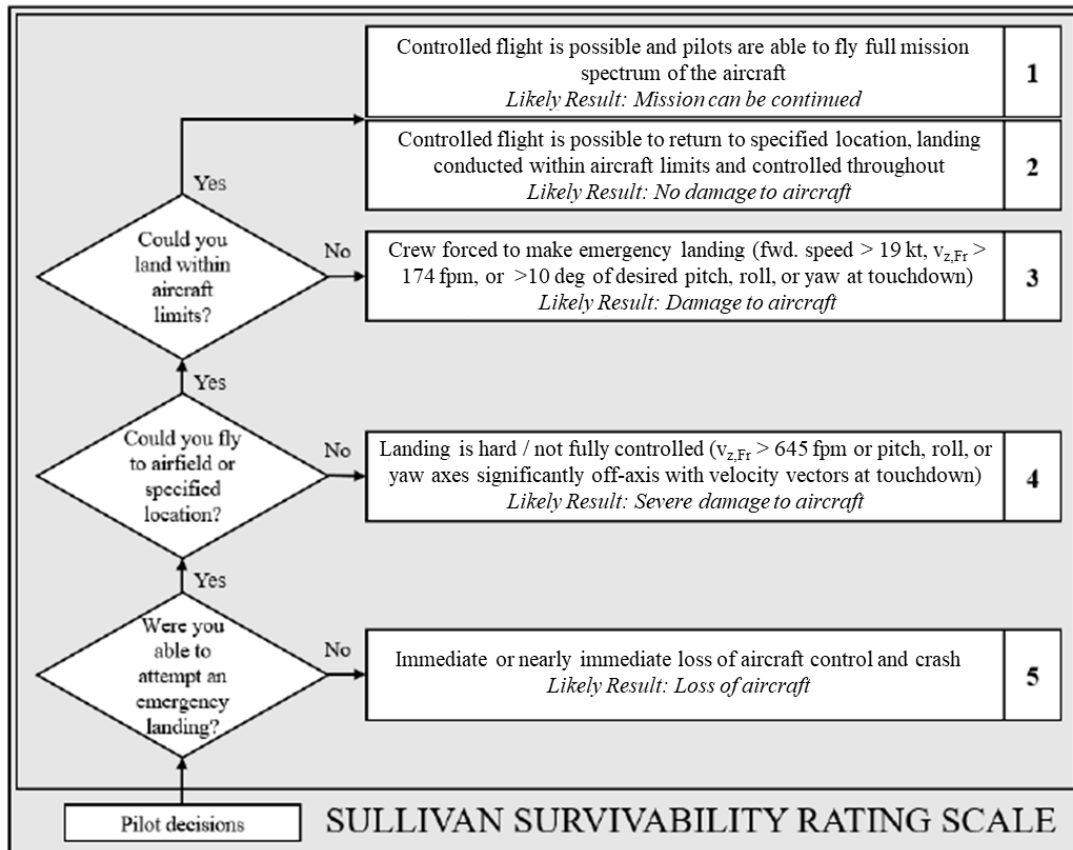


Fig. 21. Version of the Sullivan Survivability Rating (SSR) Scale used in this study.

Integrated Failure Evaluation Scheme (IFES)

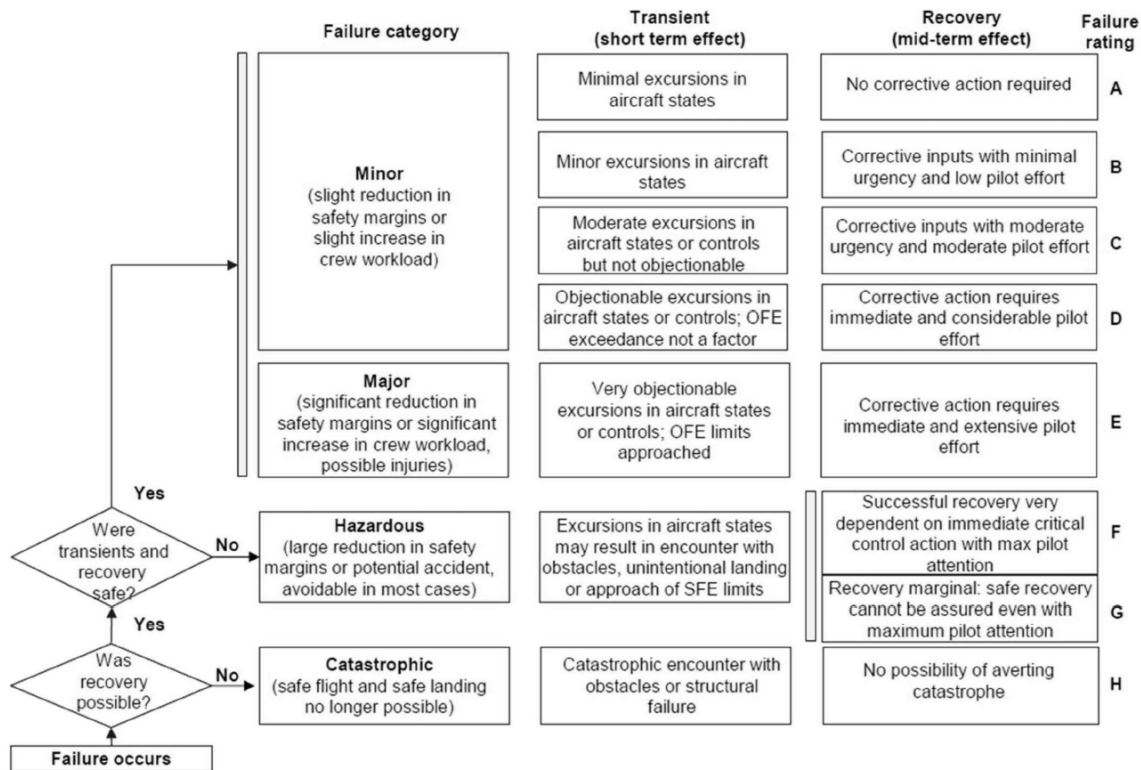


Fig. 22. The Integrated Failure Evaluation Scheme (IFES) provides an alternative, finer resolution rating scheme than the Sullivan Survivability Rating (SSR) Scale.

Results

Table 5 summarizes the SSR and IFES ratings and pilot comments and test conductor observations for each damage scenario. Overall, the results show that DTC has improved ratings and important advantages for three of the five damage scenarios tested (and little effect in the other two since the impact of the damage is very minor). Key points about the results are discussed in the following subsections.

Left Swashplate Hardover and Lockup

The left swashplate hardover and lockup (effectively a hardover at the initial control position) demonstrate the difference in the effects the amount of hardover can have on aircraft survivability and failure severity and the ability of DTC to improve it. Due to significant reallocation of control to the flaperons, DTC On achieved improvements from SSR = 5 to SSR = 3 for the hardover and from SSR = 3 to SSR = 2 for the lockup. For the IFES ratings, DTC On achieved improvements from IFES = H-H to D-B for the hardover and IFES = A-C to A-A (at high speed) for the lockup. For the lockup scenario with DTC on, note that the handling qualities degraded at low speed as the aerosurfaces became less aerodynamically effective to an IFES recovery rating of C. As previously discussed, the left swashplate hardover damage scenario is the best demonstration of the advantage provided by DTC in this study because the redundant controls have sufficient control effectiveness.

Aft Swashplate Hardover

The aft swashplate hardover DTC Off case results in a runaway condition of increasing altitude and airspeed due to the high collective position induced by the aft swashplate hardover position. In the first several tests, the pilot was unable to land the aircraft, which would likely result in loss of the aircraft. It took multiple tests for the pilot to figure out a control strategy to reduce altitude and airspeed, which involved aggressively crabbing the aircraft. Even after using this strategy, while making the final approach to the runway, lowering the collective resulted in increased speed to over 50 kt and increased altitude, which made it very difficult to achieve the final touchdown. Unintuitively, after several tests, a high collective position was found to enable the pilot to successfully land the aircraft by avoiding a significant increase in speed and allowing the aircraft to slowly descend (assuming a large runway was available). A rating of SSR = 5 and IFES = H-H was given due to the unintuitive and high workload compensation, which would likely result in loss of the aircraft.

With DTC on, the pilot was consistently able to descend and reduce speed without crabbing due to use of the flaperons and elevator to pitch and increase drag. To an unfamiliar pilot, the outcome for this case would likely be much safer than that for DTC Off and was given a rating of SSR = 3 and IFES = A-B.

Left Flaperon Hardover

The effect of the left flaperon hardover was a moderate right roll transient and slightly reduced trim speed. The aircraft could be controlled like a traditional helicopter, was landed safely, and could continue its mission (albeit with a slightly reduced top speed due to drag). Thus, this damage scenario was given a rating of SSR = 1 and IFES = C-A for the DTC On and Off cases. As previously discussed, DTC does not have a significant effect since the main rotor controls are significantly more effective than the aerosurfaces, even at 39 kt. Thus, the control allocation primarily allocates control to the main rotor servos rather than aerosurfaces with DTC on or off.

Additional tests outside of the piloted simulation study showed that it would be possible to perform a hover (rather

than run-on) landing, which is expected since the failed flaperon would not be aerodynamically effective at low speed.

Elevator Hardover

Similar to the flaperon hardover, the effect of the elevator hardover was small besides the initial transient in its primary axis of response (pitch). The aircraft could be safely landed and continue its mission and was therefore given a rating of SSR = 1 and IFES = C-A for both the DTC On and Off cases.

Additional tests outside of the piloted simulation study showed that it would be possible to perform a hover (rather than run-on) landing, which is expected since the failed elevator would not be aerodynamically effective at low speed.

Table 5. Piloted Simulation Survivability and Failure Severity Ratings for Each Damage Scenario at 39 kt

Damage Scenario	DTC	SSR	IFES	Comments
Left swashplate hardover to 5 deg (trim: 10 deg)	Off	5	H-H	<ul style="list-style-type: none"> • “Immediate” left roll and pitch down into ground • “No stick response” for recovery leading to crash shortly after
	On	3	D-B	<ul style="list-style-type: none"> • Objectionable left roll transient after damage • Beep above 35% to maintain airspeed for approach and landing • Landed 38 kt, 150 fpm (lower landing speed may be possible, but control becomes more difficult at low speed)
Left swashplate lockup	Off	3	A-C	<ul style="list-style-type: none"> • Minimal transient; roll control “softer” than normal • If speed too low, also results in poor collective control and possible high-rate descent that is difficult to compensate • Landed 16 kt, 300 ft/min (very difficult to achieve landing at low speed / low rate of descent; IFES recovery rating C for all speeds)
	On	2	A-A	<ul style="list-style-type: none"> • Minimal transient • Control “normal” at high speed (IFES recovery rating A), but degrades around 19 kt (IFES recovery rating C) • Landed 17 kt, 100 ft/min (pilot workload and control more difficult at low speed, but easier than DTC Off)
Aft swashplate hardover to 30 deg (trim: 20 deg)	Off	5	H-H	<ul style="list-style-type: none"> • Inconsistent results for this case; was only able to land safely after testing various control strategies to reduce airspeed / altitude (aggressive crabbing, adjusting beep and collective settings) • Pilot noted that an unfamiliar pilot would likely not be able to safely land aircraft
	On	3	A-B	<ul style="list-style-type: none"> • “A lot better control” at high speed; some increase in altitude and airspeed, but reduces runaway tendency compared to DTC Off • “Lack of authority at low speed; dulled collective response” • Landed 33 kt, 100 ft/min
Left flaperon hardover to 80 deg	Off	1	C-A	<ul style="list-style-type: none"> • Moderate transient causes right roll; trim airspeed is lower (~34 kt) • Control in all axes still “reasonable” • Landed comfortably within aircraft limits (14 kt, 120 ft/min)
	On	1	C-A	<ul style="list-style-type: none"> • Moderate transient causes right roll; trim airspeed is lower (~34 kt) • Landed comfortably within aircraft limits (16 kt, 130 ft/min)
Elevator hardover to 15 deg	Off	1	C-A	<ul style="list-style-type: none"> • Moderate transient in pitch axis; trim airspeed is lower (~34 kt) • Able to recover and fly normally • Landed comfortably within aircraft limits (13 kt, 150 ft/min)
	On	1	C-A	<ul style="list-style-type: none"> • Moderate transient in pitch axis; trim airspeed is lower (~34 kt) • Able to recover and fly normally • Landed comfortably within aircraft limits (13 kt, 150 ft/min)

FLIGHT-TEST EVALUATION OF DTC

Flight tests were performed at Kolb private airport in Phoenixville, PA, which has a 3,200 ft runway as shown in Fig. 23. The pilot flies line-of-sight for hover-only flights and using first-person view (FPV) goggles during flights requiring higher speeds and distances. Since the runway has a hill, only about half of the runway was used to maintain line-of-sight in case of loss of the FPV video feed.

First Hover

During the first hover flight test, the pilot's primary comment was that the aircraft was "easier to fly" and "very stable" with the new control laws. This is attributed to the explicit model-following (EMF) control architecture, ACAH response type for pitch and roll, RCAH and RCHH for collective and yaw, and parameters optimized to meet a comprehensive set of stability and performance requirements. The legacy control system had used a PID control architecture, rate response type for pitch, roll, and yaw, direct collective control, and manually tuned gains.

Control Validation

The control laws were validated periodically after major updates to the control system including the Baseline control laws at hover and 39 kt and the final DTC laws at hover and 39 kt.

Frequency sweeps were used to obtain broken- and closed-loop frequency responses from flight-test data, which are sufficient to validate the control system since they cover both the feedback and feedforward paths. Errors are easier to identify in the broken-loop frequency responses since each consists of the combined bare-airframe and control system feedback loop for each axis with the remaining feedback loops closed. Additionally, the control system acts to reduce errors in the closed-loop frequency responses to achieve good model-following. These responses were also used to compare key control system stability and performance metrics such as gain and phase margin and bandwidth and phase delay, which were used as specifications for control design in CONDUIT®. Disturbance frequency responses could also be obtained to calculate disturbance rejection bandwidth (DRB) and disturbance rejection peak (DRP) but were dropped from the flight-test plan due to time constraints. Figure 24 shows a notional block diagram with the key inputs and outputs for each frequency sweep.

Figure 25 shows the control validation results for the final DTC laws at 39 kt, which was the primary condition of importance for flight-test evaluation of DTC in this study. As discussed in Ref. 13, a frequency-domain mismatch cost $J < 100$ over the frequency range of high coherence is typically desirable to validate the control system. The broken-loop response slightly exceeds this guideline, which could be due to bare-airframe modeling errors from system identification and reduced coherence at low frequency. However, the frequency responses are generally still within the maximum unnoticeable added dynamics (MUAD) bounds, which indicates that the differences would not be perceived by the

pilot. The gain and phase margin and bandwidth and phase delay metrics obtained from the flight data match well with the results from CONDUIT® and meet Level 1 requirements as designed.

Damage Scenarios

The damage scenarios selected for flight test were evaluated carefully for safety and were only tested with DTC on since some damage scenarios with DTC off were shown to be unrecoverable in simulation. A buildup approach was used to mitigate risk and ensure that the hardovers did not result in unexpected or unsafe behavior. For safety and simplicity, the pilot used a single switch to engage and disengage the loaded DTC and damage setting. During flight testing, the DTC and damage setting was only engaged for 10-20 sec due to the short length of the airfield and to leave margin for the transient in the opposite direction after disengaging. After the damage was triggered and DTC detected the damage and automatically engaged, the pilot was instructed to test control in each axis at 39 kt (e.g. using doublets) and provide evaluation comments. The full emergency landing mission used in the piloted simulation study was not performed since run-on landings would require more careful consideration for possible updates to the landing gear and increased risk of damaging the aircraft.

Left Flaperon Hardover

DTC tests were first performed for left flaperon hardovers to 20, 40, 60, and 80 deg since it was shown in simulation to be an innocuous damage scenario, but still allowed checkout of the damage and DTC logic.

Figure 26 shows the flight test results for the left flaperon hardover to 80 deg during flight test. The damage was properly triggered such that the flaperon was commanded to the hardover position at the actuator rate limit. As expected, a small right roll transient results, but its magnitude (5 deg) is reduced relative to simulation (16 deg). The transient magnitude for the left swashplate actuator is also reduced to 6 deg from 14 deg in simulation. The reduced transient magnitudes may be due to nonlinear stall effects on the flaperons at high angles of deflection, which were not modeled.

After the transient, the pilot proceeded to test control in each axis to confirm that control was normal as expected for this damage scenario. The pilot gave an IFES rating of B-A due to the reduced transient, but similar controllability in the new steady-state compared with simulation.

Left Swashplate Hardover

More careful consideration was required for flight testing the left swashplate hardover damage scenario. In simulation it was found that the control system was robust to the initial transient, however, larger deviations in the hardover position from the trim control position (e.g. 10 to 0 deg instead of 10 to 5 deg) would cause the redundant aerosurfaces to saturate and result in loss of control after several seconds. These findings allowed the team to mitigate risk by verifying the left

swashplate trim position in flight and only implementing a hardover resulting in a change of 5 deg from this trim position (from 11 to 6 deg in flight instead of 10 to 5 deg). The tests were performed by building up the change in position implemented by the left swashplate hardover to 11, 9, 7, and 6 deg. The hardover to 6 deg represents a damage scenario that would, based on simulation, be expected to cause loss of the aircraft with DTC off, but is recoverable with DTC on.

Figure 27 shows the flight-test results for the left swashplate hardover to 6 deg. The results demonstrate that DTC was able to compensate for the initial transient and the aircraft and

actuator responses are qualitatively and quantitatively similar to those in simulation. The magnitudes of the transients in the aircraft states are 10 deg roll left, 7 deg pitch down, and 5 m/s vertical descent (compared with 12 deg roll left, 10 deg pitch down, and 5 m/s vertical descent in simulation). The magnitude of the left flaperon transient is 31 deg (compared with 27 deg in simulation). The pilot commented that the collective was not as responsive, but roll, pitch, and yaw control seemed “normal,” similar to simulation. An IFES rating of D-B was given due to the similar transient magnitudes and steady-state controllability compared with simulation.

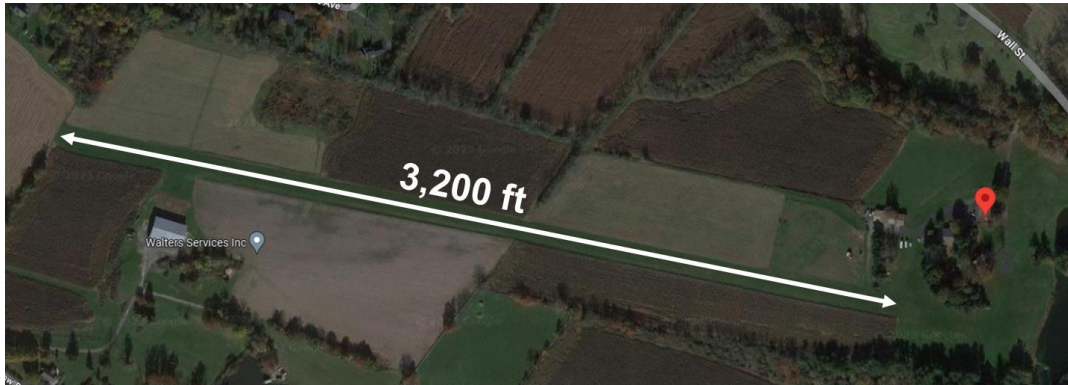


Fig. 23. Kolb private airfield in Phoenixville, PA was used for control validation and DTC flight tests.

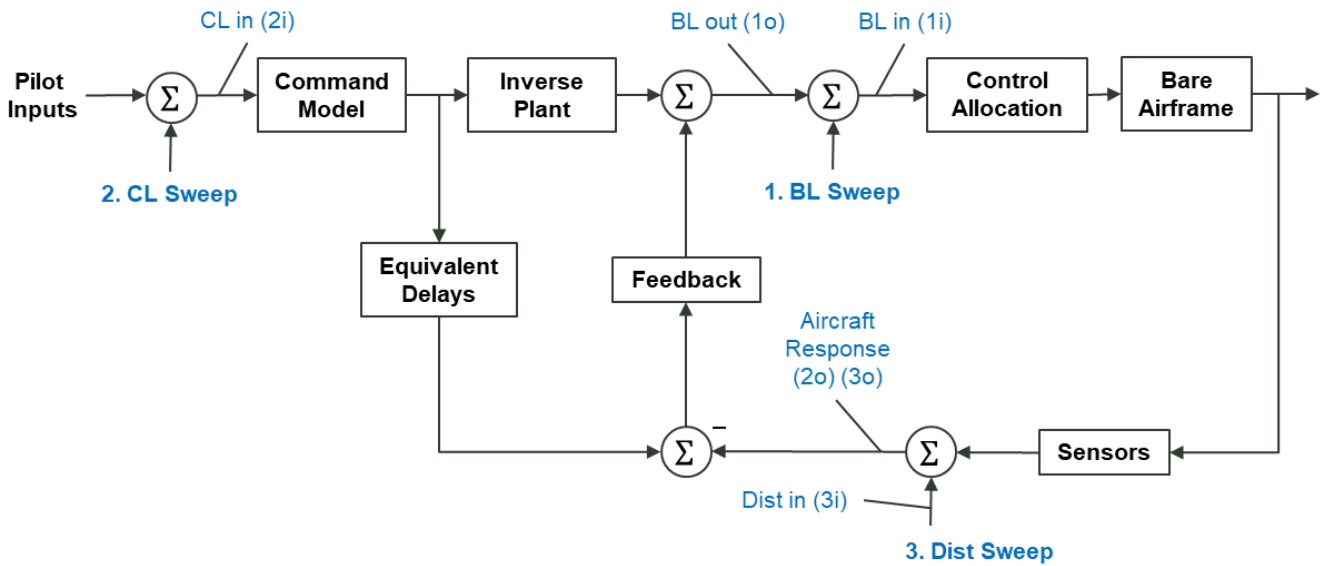


Fig. 24. Notional block diagram with location of frequency sweep inputs and outputs for control validation.

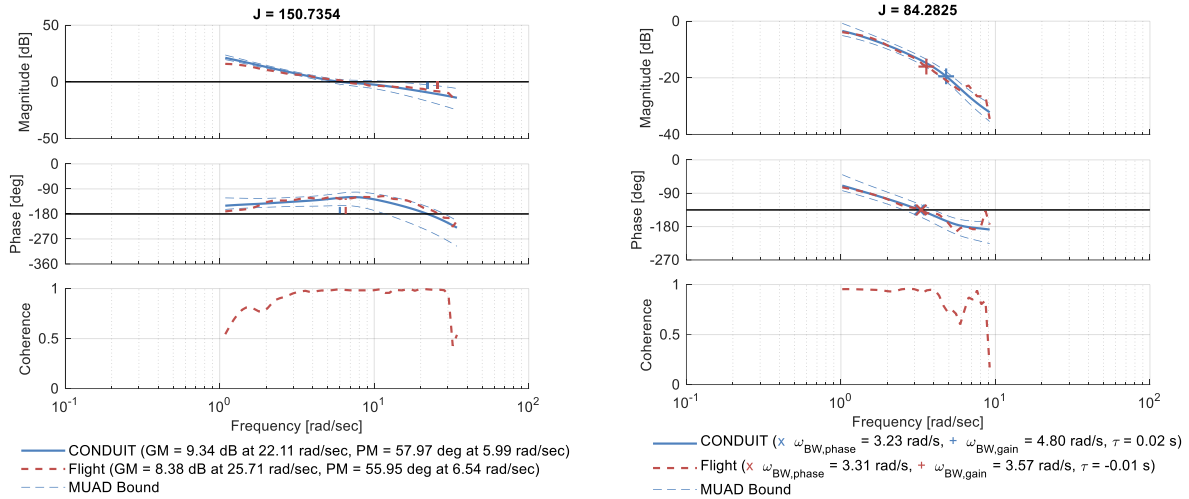


Fig. 25. Validation of the broken-loop (left) and closed-loop (right) frequency responses at 39 kt.

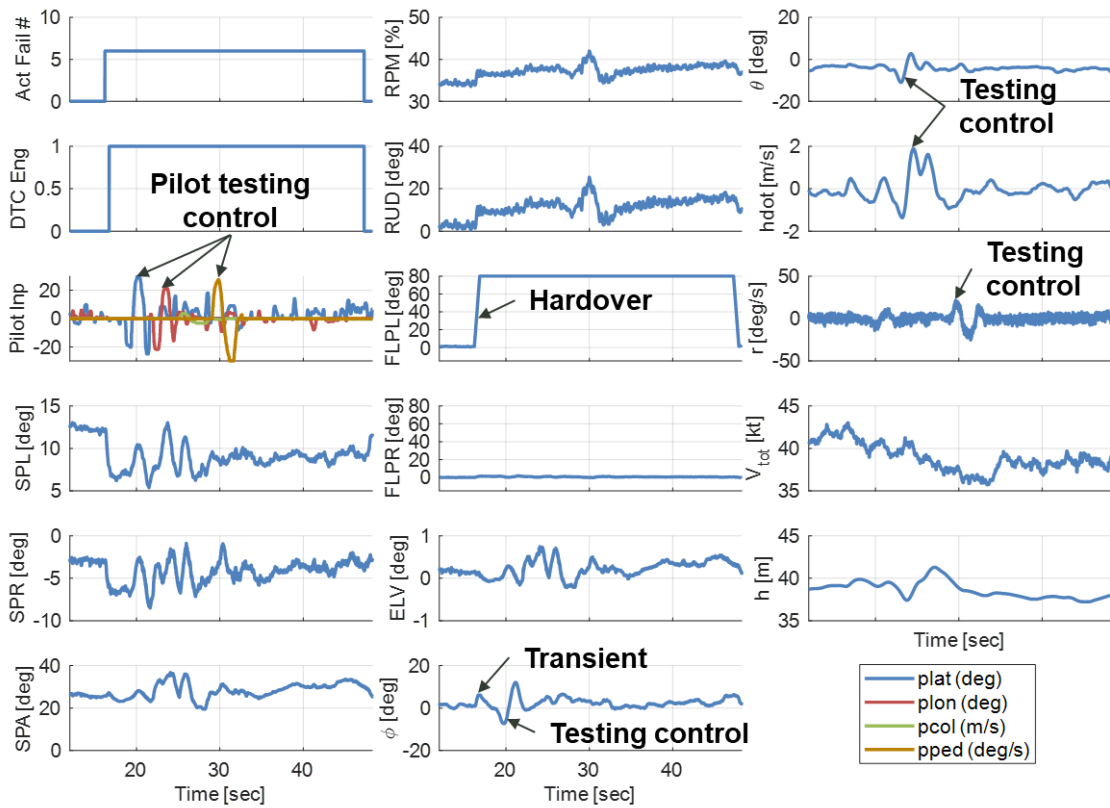


Fig. 26. Actuator and aircraft responses to left flaperon hardover to 80 deg during flight test.

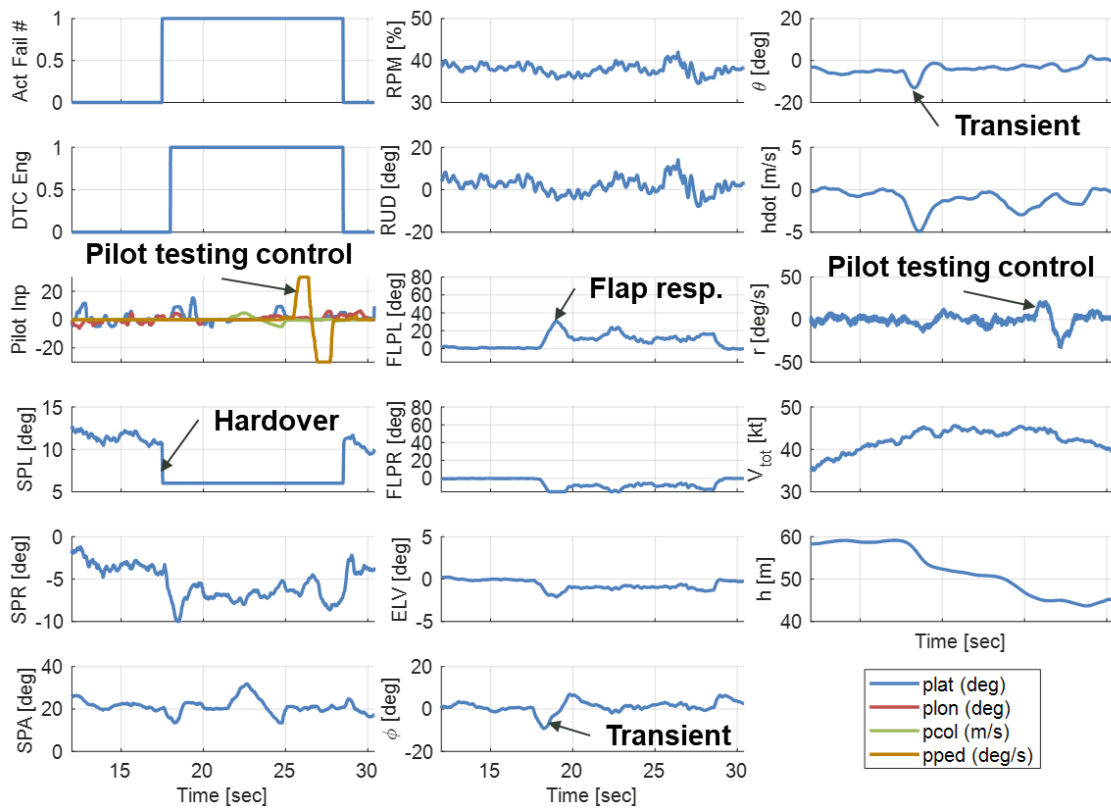


Fig. 27. Actuator and aircraft responses to left swashplate hardover to 6 deg during flight test.

LESSONS LEARNED

There were a few lessons learned from this study that may be useful to consider for other subscale and full-scale flight-test programs.

Simulation

Simulation was a valuable tool for developing and testing the control laws ahead of flight test. It also enabled the pilot to build familiarity with the new control laws using the same hardware (Taranis radio transmitter) and software (final flight-test implementation of the control laws) as would be used in flight. Based on these pre-flight tests, sweep magnitudes for control validation were also adjusted to ensure they were qualitatively not too aggressive and would not risk overstressing the aircraft. Simulation also enabled conducting the piloted simulation study, which comprehensively evaluated various damage scenarios with DTC on and off ahead of flight test.

Notably, simulation allowed precise understanding of how the aircraft and control system would behave in flight for critical maneuvers. For example, as described in the previous section, it provided a detailed understanding of how the aircraft would behave during the left swashplate hardover damage scenario. This allowed the team to mitigate risk by verifying the left swashplate trim position in flight and only implementing a hardover resulting in a change of 5 deg from this trim position (from 11 to 6 deg instead of 10 to 5 deg).

Buildup Approach

A buildup approach was used to incrementally develop and test new aspects of the control system. The Baseline control laws tested the new EMF architecture and gains, but leveraged the original Piasecki mixer and beep schedule, ahead of fully replacing them with the DTC control allocation scheme. Additionally, the scope of new control system capabilities was reduced to rely on validated signals (barometric altitude rather than radar altitude and GPS ground speed rather than airspeed) as discussed in a previous section.

A buildup approach was also used for flight test. Before each flight test, all maneuvers to be performed were tested thoroughly by the pilot in simulation. For flight test, the Baseline control laws were first tested in hover, transition, and then 39 kt during flight envelope expansion. Control validation sweeps were used throughout to quantitatively check that the control system stability and performance metrics in flight matched those expected from control design.

Flight envelope expansion was also performed for the DTC laws covering hover, transition, and 39 kt. Additionally, DTC tests were first done for left flaperon hardovers to 20, 40, 60, and 80 deg since it was shown in simulation to be an innocuous damage scenario, but still allowed checkout of damage and DTC logic. These tests were followed by buildup of the left swashplate hardover, which was a higher risk damage scenario, from 11 deg trim to 11, 9, 7, and 6 deg.

Observations About the Rating Scales

Based on the experience using the Sullivan Survivability Rating (SSR) Scale and Integrated Failure Evaluation Scheme (IFES) in this study, a few key tradeoffs were observed by the authors and are summarized herein.

The SSR Scale was found to be useful for providing an overall evaluation of the aircraft survivability across the full emergency landing mission, with clear requirements for landing within the aircraft limits. Ensuring the accuracy of the aircraft limits by in-depth analysis and testing would be beneficial for giving an accurate rating.

The IFES was found to be useful in that it provides a finer resolution scale compared with the SSR Scale and enables the pilot to give more detailed ratings that evaluate both the initial transient resulting from the failure and the subsequent recovery. However, since only a single rating is given for recovery, the IFES was not well equipped to capture variability in pilot effort across multiple flight conditions. For example, during the left swashplate hardover and lockup scenarios, the aircraft became much more difficult to fly when attempting to reduce speed for landing due to the reduced control effectiveness of the redundant aerosurfaces. These flying qualities had to instead be captured in the pilot comments.

Considerations for Flight Testing DTC

There are a few factors that are important to consider when moving from testing DTC in simulation to flight.

For safety, when flight testing the left swashplate hardover, the pilot was instructed to err on the side of activating damage at or slightly above the 39 kt speed used in simulation. This reduced risk of losing speed and redundant aerosurface control effectiveness during the damage scenario. Additionally, the pilot controls were designed such that the pilot only had to use a single switch to simultaneously activate and deactivate the loaded DTC and damage settings at will. For the left swashplate damage scenario, the pilot disengaged the damage early a couple times since the speed became too low and the redundant aerosurfaces became less effective.

Wind and gust disturbances were not modeled in simulation, but may have an important effect on the transient, actuator activity, and risk of actuator position and rate limiting. Nonlinear effects such as stall of the aerosurfaces at high angles of attack are also important to be aware of since hardovers may result in large deflections with nonlinear effects that are not captured in the system identification models. Actuator failure when the aircraft is not in trim may also be more detrimental than failures that occur when the aircraft is in trim.

Another important consideration for future work on DTC is to ensure actuator rate limits are modeled accurately and validated in flight. This is particularly important when testing damage scenarios and DTC since these cases typically involve high actuator activity and nonlinearities such as actuator rate and position limiting. Reduced rate limits would

reduce the magnitude of the transient resulting from a hardover. However, for damage scenarios such as the left swashplate hardover that rely on the redundant aerosurfaces, reduced rate limits may cause control challenges at low speed where higher aerosurface actuator activity would be demanded to compensate for their reduced aerodynamic effectiveness. Since measurements of the true actuator positions were not available during flight test in this study, it was not possible to measure the true rate limits in flight but would be important for future development and testing of DTC.

CONCLUSIONS

This work supports the following conclusions:

1. New control laws were designed for the Scaled Demonstrator that resulted in an aircraft that was “easier to fly” and “very stable” compared to the legacy control system. This is attributed to the explicit model-following (EMF) control architecture, ACAH response type for pitch and roll, RCAH and RCHH for collective and yaw, and parameters optimized to meet a comprehensive set of stability and performance requirements. The legacy control system had used a PID control architecture, rate response type for pitch, roll, and yaw, direct collective control, and manually tuned gains.
2. Damage tolerant control (DTC) was successfully implemented using a pseudo-inverse control allocation scheme and logic that enabled it to automatically engage and reallocate control based on detected damage.
3. DTC resulted in improved survivability and reduced failure severity, as measured by SSR and IFES ratings, for three of the five damage scenarios tested in the piloted simulation study. Most notably, DTC enabled recovery after a left swashplate servo hardover that was unrecoverable with DTC off. DTC for this damage scenario was successfully demonstrated in flight.
4. The effectiveness of DTC is directly related to the effectiveness of the redundant controls across all flight conditions. The effectiveness of redundant controls should be carefully considered in the preliminary design of aircraft configurations for which control redundancy is desired.
5. Lessons learned from this study were summarized. A flight-validated simulation model was essential for thoroughly testing and evaluating control system performance and behavior for various damage scenarios before proceeding to flight test.

ACKNOWLEDGEMENTS

The authors would like to acknowledge the Piasecki flight-test team, who was instrumental in ensuring a safe and successful flight-test program as required for this work. Nick Kuhn and Tom Schmidt led flight-test preparations and execution. Buz Conover and Fred Piasecki provided program management and guidance. Weiliang Dai of Universities

Space Research Association (USRA) provided support using the RIPTIDE desktop simulation environment and developed a custom head-up display (HUD) for the Scaled Demonstrator. Brian Fujizawa of DEVCOM AvMC provided useful insights on landing routes and flight-test programs.

REFERENCES

1. “Adaptive Digital Automated Pilotage Technology (ADAPT™),” Piasecki Aircraft Corporation, <https://piasecki.com/projects/adaptive-digital-automated-pilotage-technology-adapt/2726/>. Accessed 17 Sep 2021.
2. Knapp, Marit E., Ivler, Christina, M., Horn, Joseph F., Johnson, Eric N., Bridges, Derek O., Lopez, Mark J. S., Tischler, Mark B., Wagster, Joseph A., Cheung, Kenny K., “Development and Simulation of Damage Tolerant Control Laws for a Compound Helicopter,” AIAA SciTech, Orlando, FL, Jan 6-10, 2020.
3. Bridges, D. O., Berger, T., Horn, J. F., Hagwood, D. G., “Piloted Evaluation of Adaptive Flight Controls Designed to Improve Performance, Safety, and Survivability for Advanced VTOL Aircraft,” presented at the VFS Modern Ops with Future Integrated VMS Technical Meeting, West Chester, PA, Aug. 19-20, 2021.
4. Nadell, S. J., Berger, T., Dimarco, C., Lopez, M. J. S., “System Identification and Stitched Modeling of the ADAPT™ Winged Compound Helicopter Scaled Demonstrator,” Vertical Flight Society 78th Annual Forum & Technology Display, May 10-12, 2022, Ft. Worth, Texas.
5. Tobias, E. L. and Tischler, M. B., “A Model Stitching Architecture for Continuous Full Flight-Envelope Simulation of Fixed-Wing Aircraft and Rotorcraft from Discrete-Point Linear Models,” U.S. Army AMRDEC Special Report RDMR-AF-16-01, April 2016.
6. Page, A. and Steinberg, M., “A Closed-Loop Comparison of Control Allocation Methods,” in AIAA Guidance, Navigation, and Control Conference Proceedings, Denver, Colorado, 2000.
7. Oppenheimer, M., Doman, D., and Bolender, M., “Control Allocation Approaches for Over-Actuated Systems,” in Mediterranean Conference on Control and Automation Proceedings, Ancona, Italy, 2006.
8. Ivler, C. and Juhasz, O., “Evaluation of Control Allocation Techniques for a Medium Lift Tilt-Rotor,” AHS 71st Annual Forum, Virginia Beach, Virginia, May 5-7, 2015.
9. Vayalali, P., McKay, M., Gandhi, F., “Redistributed Pseudoinverse Control Allocation for Actuator Failure on a Compound Helicopter,” VFS International 76th Annual Forum & Technology Display, Virginia Beach, Virginia, October 6-8, 2020.
10. McKay, M., Vayalali, P., Gandhi, F., Berger, T., and Lopez, M. J. S., “Redistributed Allocation for Flight Control Failure on a Coaxial Helicopter,” Vertical Flight Society’s 77th Annual Forum & Technology Display, Virtual, May 10-14, 2021.
11. Lehman, R., Ceelen, S., “A Study of the Influence of Motor-ESC Dynamics on Multi Rotor Vehicle Disturbance Rejection,” Vertical Flight Society’s 78th Annual Forum & Technology Display, Ft. Worth, TX, USA, May 10-12, 2022.
12. Padfield, G. D., *Helicopter Flight Dynamics*, Wiley, 3rd Ed., p. 600, Hoboken, NJ, 2018.
13. Tischler, M. B., Berger, T., Ivler, C. M., Mansur, M. H., Cheung, K. K., and Soong, J. Y., *Practical Methods for Aircraft and Rotorcraft Flight Control Design: An Optimization-Based Approach*, AIAA Education Series, 2017.
14. Ivler, C. M., Truong, K., Kerwin, D., Otomize, J. Parmer, D., Tischler, M. B., and Gowans, N., “Development and Flight Validation of Proposed Unmanned Aerial System Handling Qualities Requirements,” Vertical Flight Society’s 76th Annual Forum & Technology Display, October 6-8, 2020.
15. Duke, E. L., Antoniewicz, R. F., and Krambeer, K. D., *Derivation and Definition of a Linear Aircraft Model*, NASA Reference Publication 1207, p. 20, August 1988.
16. Hindson, W. S., Eshow, M. M., and Schroeder, J. A., “A Pilot Rating Scale for Evaluating Failure Transients in Electronic Flight Control Systems,” AIAA-90-2827-CP, Proceedings of the AIAA Atmospheric Flight Mechanics Conference, Portland, OR, August 20-22, 1990.
17. Jones, M. and Barnett, M., “Active Inceptor Failure as a Trigger for Pilot-Induced Oscillations,” *Journal of The American Helicopter Society*, Vol. 65, No. 14, p. 1-14, 2020.
18. Anon. “Operator’s Manual for UH-60A Helicopter, UH-60L Helicopter, EH-60A Helicopter,” TM 1-1520-237-10, Headquarters, Department of the Army, October 31, 1996.